Efficient and Accurate Modeling of Planar Anisotropic Microwave Structures by the Method of Lines

Reinhold Pregla, *Fellow, IEEE*

***Abstract*—A new algorithm for the analysis of planar microwave structures with anisotropic substrates is proposed and substantiated. This algorithm is based on generalized transmission-line (GTL) equations, which are developed here for numerical algorithms. For the purpose of analysis, two different modal matrices for the discretized transverse electric and magnetic fields are calculated. Furthermore, impedance/admittance transformation formulas are developed with the help of the GTL equations for longitudinal sections and general junctions. Crossed discretization lines are used in the latter case. The materials are assumed to be biaxial or specific anisotropic. Special algorithms are developed for junctions consisting of more than two waveguides in the cross section and for bends. The proposed algorithm is verified by numerical results.**

***Index Terms*—Anisotropic materials, generalized transmission-line equations, impedance/admittance transformation, method of lines, microstrip junctions.**

I. Introduction

ONLY IN special cases do microwave and millimeter-wave devices such as integrated circuits have a simple form. Examples of complex planar circuits are shown in Fig. 1. The first one is a microstrip band-stop filter. This special structure contains various propagation paths from input to output and allows the formation of phase or group delay characteristics. The second shows a bandpass filter in coplanar-line technology featuring big differences in the dimensions. The distances of the two parts of the inner line are very small compared to the length. The proposed algorithm is very suitable for this structure because the longitudinal direction is determined analytically, whereas the cross section can be described optimally by a nonequidistant discretization scheme. As a last example, the sketch of a microstrip meander line is shown. Meander lines are especially useful as group delay equalizers or as delay elements. Here also are big differences in the dimensions. Furthermore, many lines are coupled with each other. In general, not only do the metallizations have a complex form, but also the substrates may be multilayered and the materials may have biaxial or specific anisotropic properties.

The analysis of microstrip discontinuities with bianisotropic substrates using the method of lines (MoL) [1], with discretization lines perpendicular to the surface, is given in [2]. Since the discretization is in the propagation direction, the algorithm is not suitable and adequate for devices consisting of many concatenated waveguide sections.

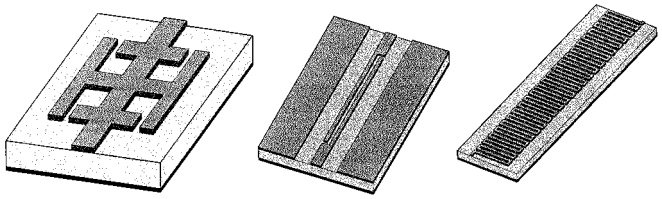

(a) (b) (c)

Fig. 1. Planar microwave circuits. (a) Band-stop filter. (b) Coplanar-line filter. (c) Meander line.

In general, microwave circuits can be described as concatenations of longitudinally homogeneous waveguide segments and junction regions. This paper aims at presenting an analysis algorithm adequate for the above-mentioned structures on anisotropic substrates. To describe the field propagation along the waveguide segments, generalized transmission-line (GTL) equations [3] for the transverse electric and magnetic fields are developed here in a special form best suited for numerical algorithms. These equations are analogous to the well-known transmission-line equations for coupled transmission lines in inhomogeneous media [4].

The GTL equations allow the normalization of the fields by using two modal matrices for the transverse electric and magnetic fields. Generally, the analysis is based on impedance/admittance transformations from the loads to the input. These transformation equations are obtained with the help of the GTL equations. The fields can be calculated in opposite direction starting at the input and proceeding to the load. This is a numerically stable algorithm. The relation between the fields at the ends of the longitudinal sections is described by a transformation of relevant impedance/admittance matrices. At the concatenations of different waveguide sections, the matching process of the fields is also performed by an impedance/admittance transformation. Waveguide junctions are analyzed with crossed discretization lines. The relations between the fields at the ports are described by open-circuit matrix parameters (short-circuit matrix parameters are also useful in some cases). Therefore, it is possible to transform again the load impedances to the input port to which the source is connected.

Algorithms based on GTL equations and in other coordinate systems have also been developed for the analysis of circuits in integrated optics [5], optical fiber structures [6], and

Manuscript received March 2, 2001; revised October 10, 2001.

The author is with the Department of Electrical Engineering, FernUniversität, D-58084 Hagen, Germany (e-mail: R.Pregla@FernUni-Hagen.de).

Publisher Item Identifier S 0018-9480(02)05209-2.

conformal antennas [7]. Eigenmode solvers for double-layered anisotropic substrates have been reported in [8] and for multilayered anisotropic waveguides by the author in [9]–[11].

The proposed algorithm will be substantiated by numerical results.

II. Basic Theory

In this section, we derive the GTL equations that are analogous to the well-known equations for coupled multiconductor transmission lines in inhomogeneous media [4] as follows:

$$\frac{d}{dz}[U] = -j[\omega L][I]$$
$$\frac{d}{dz}[I] = -j[\omega C][U]. \tag{1}$$

These equations are solved by calculating modal matrices [4], which we would also like to determine here.

A. Material Properties

For the formulation of GTL equations, the material parameters are assumed of the following form:

$$\overleftrightarrow{\nu}_r = \begin{bmatrix} \nu_{xx} & \nu_{xy} & 0 \\ \nu_{yx} & \nu_{yy} & 0 \\ 0 & 0 & \nu_{zz} \end{bmatrix}, \qquad \text{with } \nu = \varepsilon \text{ or } \mu. \tag{2}$$

The propagation takes place in the z-direction. The device under study is divided into homogeneous sections in the direction of propagation. Hence, the material parameters in the cross sections are functions of x and y only.

B. GTL Equations

GTL equations can be derived in general orthogonal coordinate system [7]. Here, we will describe the Cartesian case. Using the abbreviations

$$\hat{E} = \left[E_y, E_x\right]^t$$
$$\hat{H} = \left[-\tilde{H}_x, \tilde{H}_y\right]^t \tag{3}$$

we obtain induction of the expressions

$$\frac{\partial}{\partial \bar{z}}\hat{H} = -j[R_E]\hat{E}$$
$$\frac{\partial}{\partial \bar{z}}\hat{E} = -j[R_H]\hat{H} \tag{4}$$

from Ampere's law and the law with

$$[R_E] = \begin{bmatrix} \varepsilon_{yy} + D_{\bar{x}}\mu_{zz}^{-1}D_{\bar{x}} & \varepsilon_{yx} - D_{\bar{x}}\mu_{zz}^{-1}D_{\bar{y}} \\ \varepsilon_{xy} - D_{\bar{y}}\mu_{zz}^{-1}D_{\bar{x}} & \varepsilon_{xx} + D_{\bar{y}}\mu_{zz}^{-1}D_{\bar{y}} \end{bmatrix} \tag{5}$$

$$[R_H] = \begin{bmatrix} \mu_{xx} + D_{\bar{y}}\varepsilon_{zz}^{-1}D_{\bar{y}} & \mu_{xy} + D_{\bar{y}}\varepsilon_{zz}^{-1}D_{\bar{x}} \\ \mu_{yx} + D_{\bar{x}}\varepsilon_{zz}^{-1}D_{\bar{y}} & \mu_{yy} + D_{\bar{x}}\varepsilon_{zz}^{-1}D_{\bar{x}} \end{bmatrix}. \tag{6}$$

$D_{\bar{x},\bar{y}}$ are abbreviations for $\partial/\partial\bar{x}, \bar{y}$. The coordinates $\bar{x}, \bar{y}, \bar{z}$ are normalized with the free-space wavenumber k_0 (e.g., $\bar{x} = k_0 x$). The magnetic-field components are normalized with the free-space wave impedance $\eta_0 (\tilde{H} = \eta_0 H)$. We have replaced the field components $\tilde{H}_z$ and E_z using the remaining equations of law of induction and Ampere's law, respectively, as follows:

$$j\mu_{zz}\tilde{H}_z = [-D_{\bar{x}} \quad D_{\bar{y}}]\hat{E}$$
$$j\varepsilon_{zz}E_z = [D_{\bar{y}} \quad D_{\bar{x}}]\hat{H}. \tag{7}$$

Combining (4), we obtain

$$\frac{\partial^2}{\partial \bar{z}^2}\begin{bmatrix} E_y \\ E_x \end{bmatrix} + \begin{bmatrix} Q_{11}^E & Q_{12}^E \\ Q_{21}^E & Q_{22}^E \end{bmatrix}\begin{bmatrix} E_y \\ E_x \end{bmatrix} = \begin{bmatrix} 0 \\ 0 \end{bmatrix} \tag{8}$$

where $[Q^E] = [R_H][R_E]$. Alternatively, we can write a wave equation for $\hat{H}$. The relation between these two wave equations will be discussed later.

C. Boundary Conditions

We will demonstrate the fulfilment of boundary conditions for the case of electric walls. The case of magnetic walls will be dual. At electric walls, the tangential electric-field components must be zero. Therefore, we have to first fulfill the conditions $E_x = 0$ and $E_y = 0$ at a metallic wall $y = \text{const}$ and $x = \text{const}$, respectively. This means that in $[R_E]$ for (4a), the differential (difference) operators $D_{\bar{x}}$ and $D_{\bar{y}}$ on the right-hand sides in the submatrices have to be chosen for Dirchlet boundary conditions. The difference operators on the left-hand sides in the submatrices have to be chosen for Neumann boundary conditions. Now, $\partial E_x/\partial\bar{z} = 0$ and $\partial E_y = 0$ are also fulfilled at the same walls, respectively. Therefore, by rewriting (4b), at these walls we have

$$\frac{\partial}{\partial \bar{z}}E_y = 0 = D_{\bar{y}}^{\square}\varepsilon_{zz}^{-1}\left(D_{\bar{x}}^{\circ}\tilde{H}_y - D_{\bar{y}}^{\bullet}\tilde{H}_x\right) - \left(\mu_{xx}\tilde{H}_x + \mu_{xy}\tilde{H}_y\right) \tag{9}$$

$$\frac{\partial}{\partial \bar{z}}E_x = 0 = D_{\bar{x}}^{\square}\varepsilon_{zz}^{-1}\left(D_{\bar{x}}^{\circ}\tilde{H}_y - D_{\bar{y}}^{\bullet}\tilde{H}_x\right) + \left(\mu_{yx}\tilde{H}_x + \mu_{yy}\tilde{H}_y\right). \tag{10}$$

The first term in brackets on the right-hand sides of (9) and (10) is proportional to E_z [see (7b)], which has to be zero at the metallic walls. Therefore, the differential (difference) operators on the left-hand sides of the brackets $D_{\bar{x}}^{\square}$ and $D_{\bar{y}}^{\square}$, respectively, have to be constructed for Dirichlet boundary condition. According to the discretization scheme, the differential (difference) operators $D_{\bar{y}}^{\bullet}$ and $D_{\bar{x}}^{\circ}$ in the expressions of the first brackets have the form for Neumann boundary condition. Since we have fulfilled the condition $E_z = 0$, the terms in the second brackets $\mu_{xx}\tilde{H}_x + \mu_{xy}\tilde{H}_y$ and $\mu_{yx}\tilde{H}_x + \mu_{yy}\tilde{H}_y$ also will then be zero at the corresponding walls. Therefore, we have fulfilled the conditions $B_x = 0\,(B_y = 0)$ at the wall $x = \text{const.}(y = \text{const.})$ Since $\tilde{H}_x$ and $\tilde{H}_y$ will be discretized at different points, we have to introduce interpolation matrices M. Instead of $\mu_{xy}(\mu_{yx})$, we introduce $M_x^{\diamond}M_y^{\circ}\mu_{xy}$ $(M_y^{\diamond}M_x^{\bullet}\mu_{yx})$. $M_{xy}^{\diamond}$ must have the corresponding form for Neumann boundary conditions and $M_x^{\bullet}, M_y^{\circ}$ must have the form corresponding to the Dirichlet boundary condition with extrapolation terms. The same has to be done for ϵ_{xy} and ϵ_{yx}, but without extrapolation. The result of this investigation is that the difference operators are the same as in

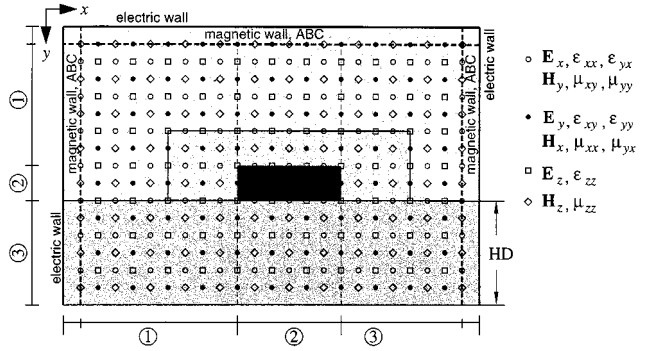

Fig. 2. Cross section of a general planar structure with discretization points.

isotropic case. We have only to use interpolation matrices with extrapolation terms. For the sake of brevity, the further discussions are restricted to the case $\nu_{xy} = \nu_{yx} = 0$.

D. Discretization of the Field and Field Equations

1) Basic Principle of Discretization: The fields and field equations will now be discretized. Discretized quantities are represented by boldface letters. Fig. 2 shows the cross section of a planar waveguide with the adequate discretization points. The field components are discretized at different points to obtain efficient formulas describing the coupling between them. $E_x(E_y)$ is determined at the same points as $H_y(H_x)$ (cf. Fig. 2). These components are required to determine the z-component of the Poynting vector in the direction of wave propagation. The discretized field components are then collected in column vectors. We order these components starting with the left-hand-side upper point going downwards along the first column. After the last point in the first column, we continue with the highest point in the second column, and so on [1]. Thus, the columns from the left- to right-hand side are put below each other. The ith column vector may be represented by a subscript i, e.g., $\mathbf{E}_{xi}$. The vector containing the collection of all these column vectors is marked by a hat (i.e., $\hat{}$) as follows:

$$\hat{\mathbf{E}}_x = \left[\mathbf{E}_{x1}^t, \mathbf{E}_{x2}^t, \ldots, \mathbf{E}_{xN_x^\circ}^t\right]^t. \tag{11}$$

If we have N_x° columns of "$\circ$" discretization points and N_y° points in each column, the total number of points is $N_y^\circ N_x^\circ$. In case of ideal metal in the cross section, the number of the discretization points in the metal area must be subtracted. If the metal is not ideal, it is considered as a dielectric with a complex permittivity. The number of "$\bullet$" columns and rows should be $N_x^\bullet$ and $N_y^\bullet$, respectively. The values of the permittivities and permeabilities are collected in the same order as the field components, not in column vectors, but in the main diagonal of a diagonal matrix. All components of the tensor are discretized on different permittivity or permeability points. Therefore, we have three different permittivity and permeability matrices, respectively. Fig. 2 shows, for example, that ε_{rx} and μ_{ry} are discretized on the same points as $\mathbf{E}_x$ and $\mathbf{H}_y$, respectively. Even in case of isotropic materials, we need three different matrices for these parameters. Hence, there is no essential difference between the algorithms for isotropic and anisotropic materials.

The differential operators are replaced by central differences. These central differences in the rows or columns are collected in the difference operators (matrices) $\boldsymbol{D}_{\bar{x}}^{\circ,\bullet}$ and $\boldsymbol{D}_{\bar{y}}^{\circ,\bullet}$, respectively, divided by the normalized discretization distances $\bar{h}_x = k_0 h_x$ and $\bar{h}_y = k_0 \bar{h}_y$, which is indicated by a bar over x and y. The collection of the difference operators [marked by a hat (i.e., $\hat{}$)] can be constructed as described in the following. In case of an inhomogeneous cross section (but without metallic subsections in it), the difference operators can be given by Kronecker products of the difference operators for the rows $(\boldsymbol{D}_x^{\circ,\bullet})$ or columns $(\boldsymbol{D}_y^{\circ,\bullet})$ and identity matrices of the order of the number of rows or columns. Accordingly, we have [1]

$$\begin{aligned} \hat{\boldsymbol{D}}_{yf}^{\circ,\bullet} &= \boldsymbol{I}_x^{\circ,\bullet} \otimes \boldsymbol{D}_y^{\circ,\bullet} \\ \hat{\boldsymbol{D}}_{xf}^{\circ,\bullet} &= \boldsymbol{D}_x^{\circ,\bullet} \otimes \boldsymbol{I}_y^{\circ,\bullet} \end{aligned} \tag{12}$$

where $\boldsymbol{I}_x^{\circ,\bullet}$ and $\boldsymbol{I}_y^{\circ,\bullet}$ are identity matrices of the order $N_x^{\circ,\bullet}$ and $N_y^{\circ,\bullet}$, respectively. The difference operators $\boldsymbol{D}_x^{\circ,\bullet}$ and $\boldsymbol{D}_y^{\circ,\bullet}$ have to fulfill Dirichlet or Neumann boundary conditions, respectively, in case of magnetic walls. In case of electric walls, the conditions have to be changed. Electric and magnetic walls have to be placed on different positions (cf. Fig. 2). If absorbing boundary conditions (ABCs) are necessary, they have to be introduced instead of magnetic walls. To be more flexible with respect to the cross section, nonequidistant discretization can also be used following the hints given in [1].

2) Matrix Reduction: In case of metallic subsections (as in Fig. 2), the discretized quantities have to be reduced. The reduction of difference operators was reported in [14]. Here, the reduction of the field vectors will be shown. The cross section should be divided with lines in vertical and horizontal directions according to the metallization boundaries. In Fig. 2, we thus obtain in both directions three different subregions. First, we assume those that have discretization points inside and on the surface of the metal. However, we would not like to use the discretized components on these points in our calculation. Therefore, we reduce the total number of discretization points to that outside the metal. Let us assume that, in our example, the number N_x° of $\circ$ columns consists of $N_{x1}^\circ, N_{x2}^\circ$, and N_{x3}° columns in the three subregions 1–3 in the x-direction, respectively. Analogously, the number N_y° of $\circ$ rows in the y-direction consists of $N_{y1}^\circ, N_{y2}^\circ$, and N_{y3}° rows in the three subregions in the y-direction. Let us define identity matrices $\boldsymbol{I}_{x1}^\circ, \boldsymbol{I}_{x2}^\circ, \boldsymbol{I}_{x3}^\circ$, $\boldsymbol{I}_{y1}^\circ, \boldsymbol{I}_{y2}^\circ$, and $\boldsymbol{I}_{y3}^\circ$ of the order $N_{x1}^\circ, N_{x2}^\circ, \ldots$, respectively. The full vector $\hat{\mathbf{F}}_f^\circ$ of the field quantity F discretized at $\circ$ points can now be reduced to the vector $\hat{\mathbf{F}}^\circ$ with components only outside the metal by

$$\hat{\mathbf{F}}^\circ = \boldsymbol{J}_\circ^t \hat{\mathbf{F}}_f^\circ \tag{13}$$

where the matrix $\boldsymbol{J}_\circ^t$ is obtained from the matrix

$$\boldsymbol{I}_x^\circ \otimes \boldsymbol{I}_y^\circ = \operatorname{diag}(\boldsymbol{I}_{x1}^\circ, \boldsymbol{I}_{x2}^\circ, \boldsymbol{I}_{x3}^\circ) \otimes \operatorname{diag}\left(\boldsymbol{I}_{y1}^\circ, \boldsymbol{I}_{y2}^\circ, \boldsymbol{I}_{y3}^\circ\right) \tag{14}$$

as

$$\boldsymbol{J}_\circ^t = \begin{bmatrix} \boldsymbol{I}_{x1}^\circ \otimes \boldsymbol{I}_y^\circ & & \\ & \boldsymbol{I}_{x2}^\circ \otimes \begin{bmatrix} \boldsymbol{I}_{y1}^\circ & \cdot & \cdot \\ \cdot & \cdot & \boldsymbol{I}_{y3}^\circ \end{bmatrix} & \\ & & \boldsymbol{I}_{x3}^\circ \otimes \boldsymbol{I}_y^\circ \end{bmatrix}. \tag{15}$$

In the middle expression, we have discarded those rows in $\boldsymbol{I}_y^\circ$, which are also rows in $\boldsymbol{I}_{y2}^\circ$. The matrices $\boldsymbol{J}_\bullet^t, \boldsymbol{J}_\square^t$, and $\boldsymbol{J}_\diamond^t$ can likewise be constructed. Now the reduced difference operators can be obtained in the following way (see also [14]):

$$\begin{aligned}\hat{\boldsymbol{D}}_x^\circ &= \boldsymbol{J}_\square^t \hat{\boldsymbol{D}}_{xf}^\circ \boldsymbol{J}_\circ \\ \hat{\boldsymbol{D}}_x^\bullet &= \boldsymbol{J}_\diamond^t \hat{\boldsymbol{D}}_{xf}^\bullet \boldsymbol{J}_\bullet \\ \hat{\boldsymbol{D}}_y^\circ &= \boldsymbol{J}_\diamond^t \hat{\boldsymbol{D}}_{yf}^\circ \boldsymbol{J}_\circ \\ \hat{\boldsymbol{D}}_y^\bullet &= \boldsymbol{J}_\square^t \hat{\boldsymbol{D}}_{yf}^\bullet \boldsymbol{J}_\bullet. \end{aligned} \tag{16}$$

We also have to reduce the diagonal matrices for the material parameters. This will be done according to

$$\begin{aligned}\hat{\boldsymbol{\epsilon}}_x &= \boldsymbol{J}_\circ^t \hat{\boldsymbol{\epsilon}}_{xxf} \boldsymbol{J}_\circ \\ \hat{\boldsymbol{\epsilon}}_y &= \boldsymbol{J}_\bullet^t \hat{\boldsymbol{\epsilon}}_{yyf} \boldsymbol{J}_\bullet \\ \hat{\boldsymbol{\epsilon}}_z &= \boldsymbol{J}_\square^t \hat{\boldsymbol{\epsilon}}_{zzf} \boldsymbol{J}_\square \\ \hat{\boldsymbol{\mu}}_x &= \boldsymbol{J}_\bullet^t \hat{\boldsymbol{\mu}}_{xxf} \boldsymbol{J}_\bullet \\ \hat{\boldsymbol{\mu}}_y &= \boldsymbol{J}_\circ^t \hat{\boldsymbol{\mu}}_{yyf} \boldsymbol{J}_\circ \\ \hat{\boldsymbol{\mu}}_z &= \boldsymbol{J}_\diamond^t \hat{\boldsymbol{\mu}}_{zzf} \boldsymbol{J}_\diamond. \end{aligned} \tag{17}$$

3) Discretized Wave Equations: With the supervectors of the discretized field components

$$\begin{aligned}\hat{\mathbf{E}} &= \left[\hat{\mathbf{E}}_y^t, \hat{\mathbf{E}}_x^t\right]^t \\ \hat{\mathbf{H}} &= \left[-\hat{\mathbf{H}}_x^t, \hat{\mathbf{H}}_y^t\right]^t \end{aligned} \tag{18}$$

discretized (4) take the form

$$\begin{aligned}\frac{d}{d\bar{z}}\hat{\mathbf{H}} &= -j\hat{\boldsymbol{R}}_E \hat{\mathbf{E}} \\ \frac{d}{d\bar{z}}\hat{\mathbf{E}} &= -j\hat{\boldsymbol{R}}_H \hat{\mathbf{H}} \end{aligned} \tag{19}$$

where

$$\hat{\boldsymbol{R}}_E = \begin{bmatrix} \hat{\boldsymbol{\epsilon}}_y - \hat{\boldsymbol{D}}_{\bar{x}}^{\bullet t} \hat{\boldsymbol{\mu}}_z^{-1} \hat{\boldsymbol{D}}_{\bar{x}}^\bullet & \hat{\boldsymbol{D}}_{\bar{x}}^{\bullet t} \hat{\boldsymbol{\mu}}_z^{-1} \hat{\boldsymbol{D}}_{\bar{y}}^\circ \\ \hat{\boldsymbol{D}}_{\bar{y}}^{\circ t} \hat{\boldsymbol{\mu}}_z^{-1} \hat{\boldsymbol{D}}_{\bar{x}}^\bullet & \hat{\boldsymbol{\epsilon}}_x - \hat{\boldsymbol{D}}_{\bar{y}}^{\circ t} \hat{\boldsymbol{\mu}}_z^{-1} \hat{\boldsymbol{D}}_{\bar{y}}^\circ \end{bmatrix} \tag{20}$$

$$\hat{\boldsymbol{R}}_H = \begin{bmatrix} \hat{\boldsymbol{\mu}}_x - \hat{\boldsymbol{D}}_{\bar{y}}^{\bullet t} \hat{\boldsymbol{\epsilon}}_z^{-1} \hat{\boldsymbol{D}}_{\bar{y}}^\bullet & -\hat{\boldsymbol{D}}_{\bar{y}}^{\bullet t} \hat{\boldsymbol{\epsilon}}_z^{-1} \hat{\boldsymbol{D}}_{\bar{x}}^\circ \\ -\hat{\boldsymbol{D}}_{\bar{x}}^{\circ t} \hat{\boldsymbol{\epsilon}}_z^{-1} \hat{\boldsymbol{D}}_{\bar{y}}^\bullet & \hat{\boldsymbol{\mu}}_y - \hat{\boldsymbol{D}}_{\bar{x}}^{\circ t} \hat{\boldsymbol{\epsilon}}_z^{-1} \hat{\boldsymbol{D}}_{\bar{x}}^\circ \end{bmatrix}. \tag{21}$$

In case of gyrotropic (gyromagnetic or gyroelectric) materials, the terms with $\epsilon_{xy}, \epsilon_{yx}, \mu_{xy}, \mu_{yx}$ must also be introduced (see Section II-C). ABCs can be realized in these equations by the following replacements:

$$\begin{aligned}\hat{\boldsymbol{D}}_{\bar{x}}^\circ &\longrightarrow \hat{\boldsymbol{D}}_{\bar{x}}^{\circ a} = \left(\boldsymbol{D}_{\bar{x}}^{\circ a} \otimes \boldsymbol{I}_y^\circ\right)_{\text{red}} \\ -\hat{\boldsymbol{D}}_x^{\bullet t} &\longrightarrow \hat{\boldsymbol{D}}_x^{\bullet a} = \left(\boldsymbol{D}_x^{\bullet a} \otimes \boldsymbol{I}_y^\bullet\right)_{\text{red}} \\ \hat{\boldsymbol{D}}_{\bar{x}}^{\circ t} &\longrightarrow \hat{\boldsymbol{D}}_{\bar{x}}^{\circ t} = \left(\boldsymbol{D}_{\bar{x}}^{\circ t} \otimes \boldsymbol{I}_y^\circ\right)_{\text{red}} \\ \hat{\boldsymbol{D}}_x^\bullet &\longrightarrow -\hat{\boldsymbol{D}}_x^{\bullet t} = -\left(\boldsymbol{D}_x^{\bullet t} \otimes \boldsymbol{I}_y^\bullet\right)_{\text{red}} \end{aligned} \tag{22}$$

where $\boldsymbol{D}_{\bar{x},\bar{y}}^{\circ a} = \boldsymbol{D}_{\bar{x},\bar{y}}^{\bullet a}$. The operators $\boldsymbol{D}_{\bar{x},\bar{y}}^{\circ,\bullet}$ correspond to $\boldsymbol{D}_{\bar{x},\bar{y}}^{\circ,\bullet a}$ (for details of ABCs in the MoL, see [16]). Equation (19) is completely analogous to the well-known equations for coupled multiconductor transmission lines [4]. Therefore, their solutions are obtained likewise. Combining (19), we obtain for the wave equations

$$\begin{aligned}\frac{d^2}{d\bar{z}^2}\hat{\mathbf{H}} - \hat{\boldsymbol{Q}}^H \hat{\mathbf{H}} &= \mathbf{0} \\ \frac{d^2}{d\bar{z}^2}\hat{\mathbf{E}} - \hat{\boldsymbol{Q}}^E \hat{\mathbf{E}} &= \mathbf{0} \end{aligned} \tag{23}$$

where

$$\begin{aligned}\hat{\boldsymbol{Q}}^H &= -\hat{\boldsymbol{R}}_E \hat{\boldsymbol{R}}_H \\ \hat{\boldsymbol{Q}}^E &= -\hat{\boldsymbol{R}}_H \hat{\boldsymbol{R}}_E \end{aligned} \tag{24}$$

and the submatrices are $(\nu_{xy} = \nu_{yx} = 0)$

$$\begin{aligned}\boldsymbol{Q}_{11}^E &= \hat{\boldsymbol{D}}_{\bar{y}}^{\bullet t} \hat{\boldsymbol{\epsilon}}_z^{-1} \hat{\boldsymbol{D}}_{\bar{y}}^\bullet \hat{\boldsymbol{\epsilon}}_y + \hat{\boldsymbol{\mu}}_x \hat{\boldsymbol{D}}_{\bar{x}}^{\bullet t} \hat{\boldsymbol{\mu}}_z^{-1} \hat{\boldsymbol{D}}_{\bar{x}}^\bullet - \hat{\boldsymbol{\epsilon}}_y \hat{\boldsymbol{\mu}}_x \\ \boldsymbol{Q}_{12}^E &= \hat{\boldsymbol{D}}_{\bar{y}}^{\bullet t} \hat{\boldsymbol{\epsilon}}_z^{-1} \hat{\boldsymbol{D}}_{\bar{x}}^\circ \hat{\boldsymbol{\epsilon}}_x - \hat{\boldsymbol{\mu}}_x \hat{\boldsymbol{D}}_{\bar{x}}^{\bullet t} \hat{\boldsymbol{\mu}}_z^{-1} \hat{\boldsymbol{D}}_{\bar{y}}^\circ \\ \boldsymbol{Q}_{21}^E &= \hat{\boldsymbol{D}}_{\bar{x}}^{\circ t} \hat{\boldsymbol{\epsilon}}_z^{-1} \hat{\boldsymbol{D}}_{\bar{y}}^\bullet \hat{\boldsymbol{\epsilon}}_y - \hat{\boldsymbol{\mu}}_y \hat{\boldsymbol{D}}_{\bar{y}}^{\circ t} \hat{\boldsymbol{\mu}}_z^{-1} \hat{\boldsymbol{D}}_{\bar{x}}^\bullet \\ \boldsymbol{Q}_{22}^E &= \hat{\boldsymbol{D}}_{\bar{x}}^{\circ t} \hat{\boldsymbol{\epsilon}}_z^{-1} \hat{\boldsymbol{D}}_{\bar{x}}^\circ \hat{\boldsymbol{\epsilon}}_x + \hat{\boldsymbol{\mu}}_y \hat{\boldsymbol{D}}_{\bar{y}}^{\circ t} \hat{\boldsymbol{\mu}}_z^{-1} \hat{\boldsymbol{D}}_{\bar{y}}^\circ - \hat{\boldsymbol{\mu}}_y \hat{\boldsymbol{\epsilon}}_x \end{aligned} \tag{25}$$

where we have taken into account that $-\boldsymbol{D}_{\bar{y}}^{\bullet t} = \boldsymbol{D}_{\bar{y}}^\circ$ and $-\boldsymbol{D}_{\bar{x}}^{\circ t} = \boldsymbol{D}_{\bar{x}}^\bullet$. Without ABCs and for biaxial anisotropy, the matrices $\hat{\boldsymbol{R}}$ are symmetric and the two $\hat{\boldsymbol{Q}}$ matrices are transposed to each other as follows:

$$\begin{aligned}\hat{\boldsymbol{R}}_{E,H} &= \hat{\boldsymbol{R}}_{E,H}^t \\ \hat{\boldsymbol{Q}}_H &= \hat{\boldsymbol{Q}}_E^t. \end{aligned} \tag{26}$$

4) Eigenvalue and Modal Matrices: Transforming the fields according to

$$\begin{aligned}\hat{\mathbf{H}} &= \hat{\boldsymbol{T}}_H \hat{\tilde{\mathbf{H}}} \\ \hat{\mathbf{E}} &= \hat{\boldsymbol{T}}_E \hat{\tilde{\mathbf{E}}}. \end{aligned} \tag{27}$$

Equation (23) reduce to

$$\begin{aligned}\frac{d^2}{d\bar{z}^2}\hat{\tilde{\mathbf{H}}} - \hat{\boldsymbol{\Gamma}}_H^2 \hat{\tilde{\mathbf{H}}} &= \mathbf{0} \\ \frac{d^2}{d\bar{z}^2}\hat{\tilde{\mathbf{E}}} - \hat{\boldsymbol{\Gamma}}_E^2 \hat{\tilde{\mathbf{E}}} &= \mathbf{0} \end{aligned} \tag{28}$$

with

$$\begin{aligned}\hat{\boldsymbol{T}}_H^{-1} \hat{\boldsymbol{Q}}_H \hat{\boldsymbol{T}}_H &= \hat{\boldsymbol{\Gamma}}_H^2 \\ \hat{\boldsymbol{T}}_E^{-1} \hat{\boldsymbol{Q}}_E \hat{\boldsymbol{T}}_E &= \hat{\boldsymbol{\Gamma}}_E^2 \\ \boldsymbol{\Gamma}_E^2 = \boldsymbol{\Gamma}_H^2 &= \boldsymbol{\Gamma}^2. \end{aligned} \tag{29}$$

Due to (24), we obtain from both eigenvalue problems in (29) identical diagonal matrices of propagation constants $\boldsymbol{\Gamma}^2$. For the solution, concepts known from other methods should be used. The general relation between the eigenvector (or modal) matrices $\hat{\boldsymbol{T}}_E$ and $\hat{\boldsymbol{T}}_H$ of $\boldsymbol{Q}_E$ and $\boldsymbol{Q}_H$, respectively, is $(\hat{\boldsymbol{\Gamma}}^2 = -\hat{\boldsymbol{\beta}}^2)$

$$\begin{aligned}\boldsymbol{T}_E &= \hat{\boldsymbol{R}}_H \boldsymbol{T}_H \hat{\boldsymbol{\beta}}^{-1} \\ \boldsymbol{T}_H &= \hat{\boldsymbol{R}}_E \boldsymbol{T}_E \hat{\boldsymbol{\beta}}^{-1} \end{aligned} \tag{30}$$

which is known from the theory of matrices. Generally, the amplitudes of the eigenvectors are free, therefore, we have intro-

duced the (diagonal) matrix $\hat{\beta}^{-1}$ for normalization. The transformation of (19) results in

$$\frac{d}{d\bar{z}}\hat{\tilde{\mathbf{E}}} = -j\hat{\beta}\hat{\tilde{\mathbf{H}}}$$
$$\frac{d}{d\bar{z}}\hat{\tilde{\mathbf{H}}} = -j\hat{\beta}\hat{\tilde{\mathbf{E}}}. \tag{31}$$

III. Impedance/Admittance Transformation

A. Transformation Through Waveguide Sections

From the general solution of (28) ($\hat{\tilde{\mathbf{F}}} = \hat{\tilde{\mathbf{E}}}, \hat{\tilde{\mathbf{H}}}$)

$$\hat{\tilde{\mathbf{F}}} = \hat{\tilde{\mathbf{F}}}_f + \hat{\tilde{\mathbf{F}}}_b = e^{-\hat{\Gamma}\bar{z}}\mathbf{A} + e^{\hat{\Gamma}\bar{z}}\mathbf{B} \tag{32}$$

we obtain for the fields in two planes A and B of a longitudinal homogeneous section whose distance is $d(\bar{d} = k_0 d)$

$$\frac{d}{d\bar{z}}\begin{bmatrix}\hat{\tilde{\mathbf{F}}}_A \\ \hat{\tilde{\mathbf{F}}}_B\end{bmatrix} = \begin{bmatrix}-\hat{\gamma} & \hat{\alpha} \\ -\hat{\alpha} & \hat{\gamma}\end{bmatrix}\begin{bmatrix}\hat{\tilde{\mathbf{F}}}_A \\ \hat{\tilde{\mathbf{F}}}_B\end{bmatrix} \tag{33}$$

$$\hat{\alpha} = \hat{\Gamma}/\sinh(\hat{\Gamma}\bar{d})$$
$$\hat{\gamma} = \hat{\Gamma}/\tanh(\hat{\Gamma}\bar{d}). \tag{34}$$

Using the first part of the general solution in (32), (the forward propagating fields $\hat{\tilde{\mathbf{F}}}_f$), we can define wave impedance/admittance matrices

$$\hat{\tilde{\boldsymbol{Z}}}_0 = \boldsymbol{I}$$
$$\hat{\tilde{\boldsymbol{Y}}}_0 = \boldsymbol{I}. \tag{35}$$

This simple result is a consequence of the field normalization using the two modal matrices $\boldsymbol{T}_E$ and $\boldsymbol{T}_H$. Introducing (31) into (33) results in

$$\begin{bmatrix}\hat{\tilde{\mathbf{H}}}_A \\ -\hat{\tilde{\mathbf{H}}}_B\end{bmatrix} = \begin{bmatrix}\hat{\bar{\boldsymbol{y}}}_1 & \hat{\bar{\boldsymbol{y}}}_2 \\ \hat{\bar{\boldsymbol{y}}}_2 & \hat{\bar{\boldsymbol{y}}}_1\end{bmatrix}\begin{bmatrix}\hat{\tilde{\mathbf{E}}}_A \\ \hat{\tilde{\mathbf{E}}}_B\end{bmatrix} \tag{36}$$

$$\begin{bmatrix}\hat{\tilde{\mathbf{E}}}_A \\ \hat{\tilde{\mathbf{E}}}_B\end{bmatrix} = \begin{bmatrix}\hat{\bar{\boldsymbol{z}}}_1 & \hat{\bar{\boldsymbol{z}}}_2 \\ \hat{\bar{\boldsymbol{z}}}_2 & \hat{\bar{\boldsymbol{z}}}_1\end{bmatrix}\begin{bmatrix}\hat{\tilde{\mathbf{H}}}_A \\ -\hat{\tilde{\mathbf{H}}}_B\end{bmatrix} \tag{37}$$

where

$$\bar{\boldsymbol{y}}_1 = \hat{\tilde{\boldsymbol{Y}}}_0/\tanh(\hat{\Gamma}\bar{d})$$
$$\bar{\boldsymbol{y}}_2 = -\hat{\tilde{\boldsymbol{Y}}}_0/\sinh(\hat{\Gamma}\bar{d})$$
$$\hat{\bar{\boldsymbol{z}}}_1 = \hat{\tilde{\boldsymbol{Z}}}_0/\tanh(\hat{\Gamma}\bar{d})$$
$$\hat{\bar{\boldsymbol{z}}}_2 = \hat{\tilde{\boldsymbol{Z}}}_0/\sinh(\hat{\Gamma}\bar{d}). \tag{38}$$

Furthermore, we also need the transfer matrix relations, which are given by

$$\begin{bmatrix}\hat{\tilde{\mathbf{E}}}_A \\ \hat{\tilde{\mathbf{H}}}_A\end{bmatrix} = \begin{bmatrix}\hat{\tilde{\boldsymbol{V}}} & \hat{\tilde{\boldsymbol{Z}}} \\ \hat{\tilde{\boldsymbol{Y}}} & \hat{\tilde{\boldsymbol{V}}}\end{bmatrix}\begin{bmatrix}\hat{\tilde{\mathbf{E}}}_B \\ \hat{\tilde{\mathbf{H}}}_B\end{bmatrix} \tag{39}$$

where

$$\hat{\tilde{\boldsymbol{V}}} = \cosh(\hat{\Gamma}\bar{d})$$
$$\hat{\tilde{\boldsymbol{Z}}} = \hat{\tilde{\boldsymbol{Z}}}_0\sinh(\hat{\Gamma}\bar{d})$$
$$\hat{\tilde{\boldsymbol{Y}}} = \hat{\tilde{\boldsymbol{Y}}}_0\sinh(\hat{\Gamma}\bar{d}). \tag{40}$$

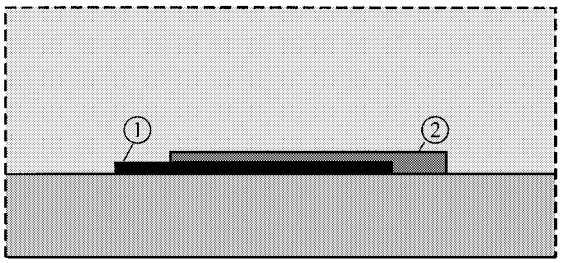

Fig. 3. Concatenation of planar waveguides 1 and 2 with different cross sections.

For the inversion only, the signs for $\hat{\tilde{\boldsymbol{Z}}}$ and $\hat{\tilde{\boldsymbol{Y}}}$ need to be changed. Defining admittances/impedances according to

$$\hat{\tilde{\mathbf{H}}}_{A,B} = \hat{\tilde{\boldsymbol{Y}}}_{A,B}\hat{\tilde{\mathbf{E}}}_{A,B}$$
$$\hat{\tilde{\mathbf{E}}}_{A,B} = \hat{\tilde{\boldsymbol{Z}}}_{A,B}\hat{\tilde{\mathbf{H}}}_{A,B} \tag{41}$$

results in the admittance/impedance transformation formulas

$$\hat{\tilde{\boldsymbol{Y}}}_A = \hat{\tilde{\boldsymbol{y}}}_1 - \hat{\tilde{\boldsymbol{y}}}_2\left(\hat{\tilde{\boldsymbol{y}}}_1 + \hat{\tilde{\boldsymbol{Y}}}_B\right)^{-1}\hat{\tilde{\boldsymbol{y}}}_2 \tag{42}$$

$$\hat{\tilde{\boldsymbol{Z}}}_A = \hat{\tilde{\boldsymbol{z}}}_1 - \hat{\tilde{\boldsymbol{z}}}_2\left(\hat{\tilde{\boldsymbol{z}}}_1 + \hat{\tilde{\boldsymbol{Z}}}_B\right)^{-1}\hat{\tilde{\boldsymbol{z}}}_2. \tag{43}$$

B. Waveguide Discontinuities

If waveguide sections with different cross sections are concatenated, the tangential fields in the common cross section have to be matched. This matching process will be explained on the example shown in Fig. 3, where two waveguides with different cross sections are concatenated. The matching process must be performed in the original domain in which the fields are given by (27). To obtain parts of the supervectors, the modal matrices must be partitioned. In a first step, the matrices $\hat{\tilde{\boldsymbol{T}}}_E$ and $\hat{\tilde{\boldsymbol{T}}}_H$ may be partitioned according to

$$\hat{\tilde{\boldsymbol{T}}}_E = \begin{bmatrix}\hat{\tilde{\boldsymbol{T}}}_{E_y} \\ \hat{\tilde{\boldsymbol{T}}}_{E_x}\end{bmatrix}$$
$$\hat{\tilde{\boldsymbol{T}}}_H = \begin{bmatrix}\hat{\tilde{\boldsymbol{T}}}_{H_x} \\ \hat{\tilde{\boldsymbol{T}}}_{H_y}\end{bmatrix} \tag{44}$$

where the number of rows in the parts is equal to the number of field components $\hat{\mathbf{E}}_y$ and $\hat{\mathbf{E}}_x$ and $\hat{\mathbf{H}}_x$ and $\hat{\mathbf{H}}_y$, respectively. The vectors of the field components in the original domain are obtained from the vectors in the transformed domain by the following relations:

$$\hat{\mathbf{E}}_x = \hat{\tilde{\boldsymbol{T}}}_{E_x}\hat{\tilde{\mathbf{E}}}$$
$$\hat{\mathbf{H}}_x = -\hat{\tilde{\boldsymbol{T}}}_{H_x}\hat{\tilde{\mathbf{H}}}. \tag{45}$$

The matrices $\hat{\tilde{\boldsymbol{T}}}_{E_x}, \hat{\tilde{\boldsymbol{T}}}_{E_y}, \hat{\tilde{\boldsymbol{T}}}_{H_x}, \hat{\tilde{\boldsymbol{T}}}_{H_y}$ may be further partitioned according to the columns of the discretization points in the cross section (see Fig. 2). If we have, for example, N_x° columns of $\circ$ discretization points then we may, for example, partition $\hat{\tilde{\boldsymbol{T}}}_{E_x}$ in N_x° submatrices, where the number of rows in each of the submatrices is equal to the number of the $\circ$ discretization points in that column. Denoting the nth submatrix of $\boldsymbol{T}_{E_x}$ for the nth

column by $\boldsymbol{T}_{E_{xn}}$, then the subvector of the field components $\mathbf{E}_x$ in the nth "$\circ$" column is given by

$$\mathbf{E}_{xn} = \boldsymbol{T}_{E_{xn}} \hat{\tilde{\mathbf{E}}}, \qquad n \in \{1, N_x^{\circ}\}. \tag{46}$$

In an analogous way, the other field components can be calculated in their columns.

In case of planar structures and two-dimensional discretization, the field matching and impedance transformation at discontinuities should also be described by a matrix partition with the help of suitable $\boldsymbol{J}$ matrices. The matching of the tangential electric field results in

$$\hat{\boldsymbol{J}}_1^m \boldsymbol{T}_{E1} \hat{\tilde{\mathbf{E}}}_1 = \mathbf{0} \tag{47}$$

$$\hat{\boldsymbol{J}}_1^c \boldsymbol{T}_{E1} \hat{\tilde{\mathbf{E}}}_1 = \hat{\boldsymbol{J}}_2^c \boldsymbol{T}_{E2} \hat{\tilde{\mathbf{E}}}_2 \tag{48}$$

$$\mathbf{0} = \hat{\boldsymbol{J}}_2^m \boldsymbol{T}_{E2} \hat{\tilde{\mathbf{E}}}_2. \tag{49}$$

The matrices $\hat{\boldsymbol{J}}_1^c (\hat{\boldsymbol{J}}_2^c)$ reduce the field $\boldsymbol{T}_{E1} \hat{\tilde{\boldsymbol{E}}}_1$ in the original domain to that part common to the field of waveguide 2 (1) and can be calculated from the $\boldsymbol{J}_{\circ,\bullet}$ matrices in Section II-C.2 by

$$\begin{aligned} \hat{\boldsymbol{J}}_1^c &= \operatorname{diag}\left(\boldsymbol{J}_{\bullet 2}^t \boldsymbol{J}_{\bullet 1}, \boldsymbol{J}_{\circ 2}^t \boldsymbol{J}_{\circ 1}\right) \\ \hat{\boldsymbol{J}}_2^c &= \operatorname{diag}\left(\boldsymbol{J}_{\bullet 1}^t \boldsymbol{J}_{\bullet 2}, \boldsymbol{J}_{\circ 1}^t \boldsymbol{J}_{\circ 2}\right). \end{aligned} \tag{50}$$

$\hat{\boldsymbol{J}}_1^m \boldsymbol{T}_{E1} \hat{\tilde{\boldsymbol{E}}}_1 (\hat{\boldsymbol{J}}_2^m \boldsymbol{T}_{E2} \hat{\tilde{\boldsymbol{E}}}_2)$ is the field part of the metallic front end of waveguide 2 (1). From (47) and (48), we obtain

$$\hat{\tilde{\mathbf{E}}}_1 = \boldsymbol{T}_{E1}^{-1} \begin{bmatrix} \hat{\boldsymbol{J}}_2^c \boldsymbol{T}_{E2} \\ \mathbf{0} \end{bmatrix} \hat{\tilde{\mathbf{E}}}_2 = \boldsymbol{T}_{E1}^{-1} \hat{\boldsymbol{J}}_1^{ct} \hat{\boldsymbol{J}}_2^c \boldsymbol{T}_{E2} \hat{\tilde{\mathbf{E}}}_2. \tag{51}$$

The matrix with the zero rows has to be understood symbolically, because these zeros are placed between the rows in the upper submatrix. Analogously we obtain from (48) and (49)

$$\hat{\tilde{\mathbf{E}}}_2 = \boldsymbol{T}_{E2}^{-1} \hat{\boldsymbol{J}}_2^{ct} \hat{\boldsymbol{J}}_1^c \boldsymbol{T}_{E1} \hat{\tilde{\mathbf{E}}}_1. \tag{52}$$

Matching the magnetic field, we obtain

$$\begin{aligned} \hat{\boldsymbol{J}}_1^c \boldsymbol{T}_{H1} \hat{\tilde{\mathbf{H}}}_1 &= \hat{\boldsymbol{J}}_2^c \boldsymbol{T}_{H2} \hat{\tilde{\mathbf{H}}}_2 \\ &= \hat{\boldsymbol{J}}_2^c \boldsymbol{T}_{H2} \hat{\tilde{\boldsymbol{Y}}}_2 \hat{\tilde{\mathbf{E}}}_2 \qquad (53) \\ &= \hat{\boldsymbol{J}}_2^c \boldsymbol{T}_{H2} \hat{\tilde{\boldsymbol{Y}}}_2 \boldsymbol{T}_{E2}^{-1} \hat{\boldsymbol{J}}_2^{ct} \hat{\boldsymbol{J}}_1^c \boldsymbol{T}_{E1} \hat{\tilde{\mathbf{E}}}_1. \qquad (54) \end{aligned}$$

The last equation may be rewritten and combined with (47) yielding

$$\begin{bmatrix} \hat{\boldsymbol{J}}_1^c \\ \hat{\boldsymbol{J}}_1^m \end{bmatrix} \boldsymbol{T}_{E1} \hat{\tilde{\mathbf{E}}}_1 = \begin{bmatrix} \left(\hat{\boldsymbol{J}}_2^c \boldsymbol{T}_{H2} \hat{\tilde{\boldsymbol{Y}}}_2 \boldsymbol{T}_{E2}^{-1} \hat{\boldsymbol{J}}_2^{ct} \right)^{-1} \hat{\boldsymbol{J}}_1^c \boldsymbol{T}_{H1} \hat{\tilde{\mathbf{H}}}_1 \\ \mathbf{0} \end{bmatrix}. \tag{55}$$

Using a procedure analogous to (51), we obtain

$$\hat{\tilde{\mathbf{E}}}_1 = \boldsymbol{T}_{E1}^{-1} \hat{\boldsymbol{J}}_1^{ct} \left(\hat{\boldsymbol{J}}_2^c \boldsymbol{T}_{H2} \hat{\tilde{\boldsymbol{Y}}}_2 \boldsymbol{T}_{E2}^{-1} \hat{\boldsymbol{J}}_2^{ct} \right)^{-1} \hat{\boldsymbol{J}}_1^c \boldsymbol{T}_{H1} \hat{\tilde{\mathbf{H}}}_1. \tag{56}$$

Therefore, the impedance is given by

$$\hat{\tilde{\boldsymbol{Z}}}_1 = \boldsymbol{T}_{E1}^{-1} \hat{\boldsymbol{J}}_1^{ct} \left(\hat{\boldsymbol{J}}_2^c \boldsymbol{T}_{H2} \hat{\tilde{\boldsymbol{Y}}}_2 \boldsymbol{T}_{E2}^{-1} \hat{\boldsymbol{J}}_2^{ct} \right)^{-1} \hat{\boldsymbol{J}}_1^c \boldsymbol{T}_{H1}. \tag{57}$$

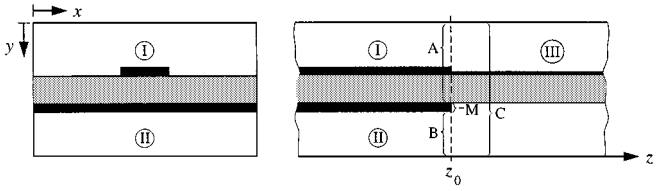

Fig. 4. Junction of three waveguides at $z = z_0$.

C. Impedance Transformation at Waveguide Junctions

In this subsection, we would like to demonstrate how waveguide junctions, as in Fig. 4, i.e., with a common cross section, can be modeled. The algorithm to be developed is suitable for the analysis of microstrip-to-rectangular waveguide transition proposed in [13]. At the common cross section of the waveguides (at $z = z_0$), the field relation in regions I–III can be written with the help of impedance matrices as follows:

$$\begin{aligned} \hat{\tilde{\mathbf{E}}}_A^{\mathrm{I}} &= \hat{\tilde{\boldsymbol{Z}}}_A^{\mathrm{I}} \hat{\tilde{\mathbf{H}}}_A^{\mathrm{I}} \\ \hat{\tilde{\mathbf{E}}}_B^{\mathrm{II}} &= -\hat{\tilde{\boldsymbol{Z}}}_B^{\mathrm{II}} \hat{\tilde{\mathbf{H}}}_B^{\mathrm{II}} \\ \hat{\tilde{\mathbf{E}}}_C^{\mathrm{III}} &= \hat{\tilde{\boldsymbol{Z}}}_C^{\mathrm{III}} \hat{\tilde{\mathbf{H}}}_C^{\mathrm{III}}. \end{aligned} \tag{58}$$

For the matching procedure, we must split the tangential electric and magnetic fields in waveguide III considering the different parts of the cross section (A, B, and M in Fig. 4). We obtain

$$\hat{\tilde{\mathbf{E}}}_C^{\mathrm{III}} = \begin{bmatrix} \hat{\tilde{\mathbf{E}}}_A^{\mathrm{III}} \\ \hat{\tilde{\mathbf{E}}}_M^{\mathrm{III}} \\ \hat{\tilde{\mathbf{E}}}_B^{\mathrm{III}} \end{bmatrix} = \begin{bmatrix} \hat{\boldsymbol{J}}_{\mathrm{III}A} \hat{\tilde{\mathbf{E}}}_C^{\mathrm{III}} \\ \hat{\boldsymbol{J}}_{\mathrm{III}M} \hat{\tilde{\mathbf{E}}}_C^{\mathrm{III}} \\ \hat{\boldsymbol{J}}_{\mathrm{III}B} \hat{\tilde{\mathbf{E}}}_C^{\mathrm{III}} \end{bmatrix} \tag{59}$$

$$\hat{\tilde{\mathbf{H}}}_C^{\mathrm{III}} = \begin{bmatrix} \hat{\tilde{\mathbf{H}}}_A^{\mathrm{III}} \\ \hat{\tilde{\mathbf{H}}}_M^{\mathrm{III}} \\ \hat{\tilde{\mathbf{H}}}_B^{\mathrm{III}} \end{bmatrix} = \begin{bmatrix} \hat{\boldsymbol{J}}_{\mathrm{III}A} \hat{\tilde{\mathbf{H}}}_C^{\mathrm{III}} \\ \hat{\boldsymbol{J}}_{\mathrm{III}M} \hat{\tilde{\mathbf{H}}}_C^{\mathrm{III}} \\ \hat{\boldsymbol{J}}_{\mathrm{III}B} \hat{\tilde{\mathbf{H}}}_C^{\mathrm{III}} \end{bmatrix}. \tag{60}$$

The subvector $\hat{\mathbf{E}}_M$ represents the electric field on the nonideal metallic end between regions A and B. In case of ideal metal, $\mathbf{E}_M$ is a vector with zero components. Again, $\hat{\boldsymbol{J}}$ are reduction matrices. With these matrices, the field components on special lines are selected and related to the different regions, e.g., $\hat{\boldsymbol{J}}_{\mathrm{III}M}$ selects the lines in region III, which end at the metal M. With all these matrices, $\hat{\boldsymbol{J}}$ for a waveguide cross section—in our case, $\hat{\boldsymbol{J}}_{\mathrm{III}A,B,M}$—a identity matrix can be formed. This procedure is equivalent to the matrix partition technique proposed in [10] and [11].

Matching the tangential electric field using the vectors in the transformed domain, we obtain

$$\boldsymbol{T}_{\mathrm{III}} \hat{\tilde{\mathbf{E}}}_C^{\mathrm{III}} = \begin{bmatrix} \hat{\boldsymbol{J}}_{\mathrm{III}A} \boldsymbol{T}_{\mathrm{III}} \\ \hat{\boldsymbol{J}}_{\mathrm{III}M} \boldsymbol{T}_{\mathrm{III}} \\ \hat{\boldsymbol{J}}_{\mathrm{III}B} \boldsymbol{T}_{\mathrm{III}} \end{bmatrix} \hat{\tilde{\mathbf{E}}}_C^{\mathrm{III}} = \begin{bmatrix} \boldsymbol{T}_{\mathrm{I}} \hat{\tilde{\mathbf{E}}}_A \\ \hat{\tilde{\mathbf{E}}}_M \\ \boldsymbol{T}_{\mathrm{II}} \hat{\tilde{\mathbf{E}}}_B \end{bmatrix}. \tag{61}$$

The vector $\hat{\tilde{\mathbf{E}}}_C^{\mathrm{III}}$ is a function of $\hat{\tilde{\mathbf{E}}}_A, \hat{\tilde{\mathbf{E}}}_B, \hat{\mathbf{E}}_M$ and is, therefore, given as

$$\hat{\tilde{\mathbf{E}}}_C^{\mathrm{III}} = \boldsymbol{T}_{\mathrm{III}}^{-1} \begin{bmatrix} \hat{\boldsymbol{J}}_{\mathrm{III}A}^t \boldsymbol{T}_{\mathrm{I}} \hat{\tilde{\mathbf{E}}}_A \\ \hat{\boldsymbol{J}}_{\mathrm{III}M}^t \hat{\mathbf{E}}_M \\ \hat{\boldsymbol{J}}_{\mathrm{III}B}^t \boldsymbol{T}_{\mathrm{II}} \hat{\tilde{\mathbf{E}}}_B \end{bmatrix} \tag{62}$$

which can be written in the following form:

$$\hat{\tilde{\mathbf{E}}}_C^{\mathrm{III}} = \boldsymbol{T}_{\mathrm{III}}^{-1}\hat{\boldsymbol{J}}_{\mathrm{III}A}^{t}\boldsymbol{T}_{\mathrm{I}}\hat{\tilde{\mathbf{E}}}_A + \boldsymbol{T}_{\mathrm{III}}^{-1}\hat{\boldsymbol{J}}_{\mathrm{III}B}^{t}\boldsymbol{T}_{\mathrm{II}}\hat{\tilde{\mathbf{E}}}_B + \boldsymbol{T}_{\mathrm{III}}^{-1}\hat{\boldsymbol{J}}_{\mathrm{III}M}^{t}\hat{\mathbf{E}}_M. \tag{63}$$

Analogously, matching the tangential magnetic field, we obtain in the transformed domain the equations

$$\boldsymbol{T}_{\mathrm{III}}\hat{\tilde{\mathbf{H}}}_C^{\mathrm{III}} = \begin{bmatrix} \hat{\boldsymbol{J}}_{\mathrm{III}A}\boldsymbol{T}_{\mathrm{III}} \\ \hat{\boldsymbol{J}}_{\mathrm{III}M}\boldsymbol{T}_{\mathrm{III}} \\ \hat{\boldsymbol{J}}_{\mathrm{III}B}\boldsymbol{T}_{\mathrm{III}} \end{bmatrix} \hat{\tilde{\mathbf{H}}}_C^{\mathrm{III}} = \begin{bmatrix} \hat{\mathbf{H}}_A \\ \hat{\mathbf{S}}_M \\ \hat{\mathbf{H}}_B \end{bmatrix} = \begin{bmatrix} \boldsymbol{T}_{\mathrm{I}}\hat{\tilde{\mathbf{H}}}_A^{\mathrm{I}} \\ \hat{\mathbf{S}}_M \\ \boldsymbol{T}_{\mathrm{II}}\hat{\tilde{\mathbf{H}}}_B^{\mathrm{II}} \end{bmatrix} \tag{64}$$

where $\hat{\mathbf{S}}_M$ is the current density on the metallic end between regions A and B, i.e., located on the same places as $\hat{\mathbf{E}}_M$. The following three equations result from this array:

$$\boldsymbol{T}_{\mathrm{I}}\hat{\tilde{\mathbf{H}}}_A^{\mathrm{I}} = \hat{\boldsymbol{J}}_{\mathrm{III}A}\boldsymbol{T}_{\mathrm{III}}\hat{\tilde{\mathbf{H}}}_C^{\mathrm{III}} \tag{65}$$

$$\boldsymbol{T}_{\mathrm{II}}\hat{\tilde{\mathbf{H}}}_B^{\mathrm{II}} = \hat{\boldsymbol{J}}_{\mathrm{III}B}\boldsymbol{T}_{\mathrm{III}}\hat{\tilde{\mathbf{H}}}_C^{\mathrm{III}} \tag{66}$$

$$\hat{\mathbf{S}}_M = \hat{\boldsymbol{J}}_{\mathrm{III}M}\boldsymbol{T}_{\mathrm{III}}\hat{\tilde{\mathbf{H}}}_C^{\mathrm{III}}. \tag{67}$$

The associated equations for tangential electric-field vectors $\hat{\tilde{\mathbf{E}}}_A$ and $\hat{\tilde{\mathbf{E}}}_B$ are obtained using (58)

$$\hat{\tilde{\mathbf{E}}}_A^{\mathrm{I}} = \hat{\tilde{\boldsymbol{Z}}}_A\boldsymbol{T}_{\mathrm{I}}^{-1}\hat{\boldsymbol{J}}_{\mathrm{III}A}\boldsymbol{T}_{\mathrm{III}}\hat{\tilde{\boldsymbol{Y}}}_C\hat{\tilde{\mathbf{E}}}_C^{\mathrm{III}} \tag{68}$$

$$\hat{\tilde{\mathbf{E}}}_B^{\mathrm{II}} = -\hat{\tilde{\boldsymbol{Z}}}_B\boldsymbol{T}_{\mathrm{II}}^{-1}\hat{\boldsymbol{J}}_{\mathrm{III}B}\boldsymbol{T}_{\mathrm{III}}\hat{\tilde{\boldsymbol{Y}}}_C\hat{\tilde{\mathbf{E}}}_C^{\mathrm{III}}. \tag{69}$$

Replacing $\hat{\tilde{\mathbf{H}}}_C$ in (65)–(67) by $\bar{\boldsymbol{Y}}_C\hat{\tilde{\mathbf{E}}}_C$ and introducing (63) into these equations, we obtain

$$\begin{bmatrix} \hat{\tilde{\mathbf{H}}}_A \\ -\hat{\tilde{\mathbf{H}}}_B \\ \hat{\mathbf{S}}_M \end{bmatrix} = \begin{bmatrix} \hat{\tilde{\boldsymbol{y}}}_{AA} & \hat{\tilde{\boldsymbol{y}}}_{AB} & \hat{\tilde{\boldsymbol{y}}}_{AM} \\ \hat{\tilde{\boldsymbol{y}}}_{BA} & \hat{\tilde{\boldsymbol{y}}}_{BB} & \hat{\tilde{\boldsymbol{y}}}_{BM} \\ \hat{\tilde{\boldsymbol{y}}}_{MA} & \hat{\tilde{\boldsymbol{y}}}_{MB} & \hat{\tilde{\boldsymbol{y}}}_{MM} \end{bmatrix} \begin{bmatrix} \hat{\tilde{\mathbf{E}}}_A \\ \hat{\tilde{\mathbf{E}}}_B \\ \hat{\mathbf{E}}_M \end{bmatrix} \tag{70}$$

where the submatrices are given with the abbreviations

$$\begin{aligned} \hat{\boldsymbol{Y}}_C &= \boldsymbol{T}_{\mathrm{III}}\hat{\tilde{\boldsymbol{Y}}}_C\boldsymbol{T}_{\mathrm{III}}^{-1} \\ \hat{\boldsymbol{Y}}_{CM} &= \hat{\boldsymbol{Y}}_C\hat{\boldsymbol{J}}_{\mathrm{III}M}^{t} \\ \hat{\boldsymbol{Y}}_{CA} &= \hat{\boldsymbol{Y}}_C\hat{\boldsymbol{J}}_{\mathrm{III}A}^{t}\boldsymbol{T}_{\mathrm{I}} \\ \hat{\boldsymbol{Y}}_{CB} &= \hat{\boldsymbol{Y}}_C\hat{\boldsymbol{J}}_{\mathrm{III}B}^{t}\boldsymbol{T}_{\mathrm{II}} \end{aligned}$$

by

$$\begin{aligned} \hat{\tilde{\boldsymbol{y}}}_{AA} &= \boldsymbol{T}_{\mathrm{I}}^{-1}\hat{\boldsymbol{J}}_{\mathrm{III}A}\hat{\boldsymbol{Y}}_{CA} \\ \hat{\tilde{\boldsymbol{y}}}_{AB} &= \boldsymbol{T}_{\mathrm{I}}^{-1}\hat{\boldsymbol{J}}_{\mathrm{III}A}\hat{\boldsymbol{Y}}_{CB} \\ \hat{\tilde{\boldsymbol{y}}}_{BA} &= -\boldsymbol{T}_{\mathrm{II}}^{-1}\hat{\boldsymbol{J}}_{\mathrm{III}B}\hat{\boldsymbol{Y}}_{CA} \\ \hat{\tilde{\boldsymbol{y}}}_{BB} &= -\boldsymbol{T}_{\mathrm{II}}^{-1}\hat{\boldsymbol{J}}_{\mathrm{III}B}\hat{\boldsymbol{Y}}_{CB} \\ \hat{\tilde{\boldsymbol{y}}}_{AM} &= \boldsymbol{T}_{\mathrm{I}}^{-1}\hat{\boldsymbol{J}}_{\mathrm{III}A}\hat{\boldsymbol{Y}}_{CM} \\ \hat{\tilde{\boldsymbol{y}}}_{BM} &= -\boldsymbol{T}_{\mathrm{II}}^{-1}\hat{\boldsymbol{J}}_{\mathrm{III}B}\hat{\boldsymbol{Y}}_{CM} \\ \hat{\tilde{\boldsymbol{y}}}_{MA} &= \hat{\boldsymbol{J}}_{\mathrm{III}M}\hat{\boldsymbol{Y}}_{CA} \\ \hat{\tilde{\boldsymbol{y}}}_{MB} &= \hat{\boldsymbol{J}}_{\mathrm{III}M}\hat{\boldsymbol{Y}}_{CB} \\ \hat{\tilde{\boldsymbol{y}}}_{MM} &= \hat{\boldsymbol{J}}_{\mathrm{III}M}\hat{\boldsymbol{Y}}_{CM}. \end{aligned} \tag{71}$$

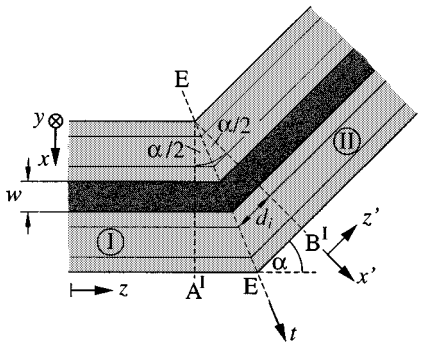

Fig. 5. Sharp microstrip bend of bend angle α.

First we consider the case of ideal material with $\hat{\mathbf{E}}_M = \mathbf{0}$. In this case, the last equation in system (70) decouples from the first one. Now with respect to (58), we obtain from the second equation in the system (70)

$$\begin{aligned} \hat{\tilde{\mathbf{E}}}_B &= -(\hat{\tilde{\boldsymbol{y}}}_{BB} - \hat{\tilde{\boldsymbol{Y}}}_B)^{-1}\hat{\tilde{\boldsymbol{y}}}_{BA}\hat{\tilde{\mathbf{E}}}_A \\ \hat{\tilde{\boldsymbol{Y}}}_B &= \hat{\tilde{\boldsymbol{Z}}}_B^{-1} \end{aligned} \tag{72}$$

which may be introduced into the first equation in (70)

$$\hat{\tilde{\mathbf{H}}}_A = \left(\hat{\tilde{\boldsymbol{y}}}_{AA} - \hat{\tilde{\boldsymbol{y}}}_{AB}\left(\hat{\tilde{\boldsymbol{y}}}_{BB} - \hat{\tilde{\boldsymbol{Y}}}_B\right)^{-1}\hat{\tilde{\boldsymbol{y}}}_{BA}\right)\hat{\tilde{\mathbf{E}}}_A = \hat{\tilde{\boldsymbol{Y}}}_A\hat{\tilde{\mathbf{E}}}_A. \tag{73}$$

The admittance $\hat{\tilde{\boldsymbol{Y}}}_A$ is, therefore, given by

$$\hat{\tilde{\boldsymbol{Y}}}_A = \hat{\tilde{\boldsymbol{y}}}_{AA} - \hat{\tilde{\boldsymbol{y}}}_{AB}\left(\hat{\tilde{\boldsymbol{y}}}_{BB} - \hat{\tilde{\boldsymbol{Y}}}_B\right)^{-1}\hat{\tilde{\boldsymbol{y}}}_{BA} \tag{74}$$

which has the same form as (42) and (43).

In case of a nonideal metal wall, the approximate boundary conditions for the tangential fields on the metallic surface $\eta_m\vec{H}_t = \vec{e}_z \times \vec{E}_t$ can be used. Assuming waveguide I is excited by the fundamental mode, then the field $\hat{\tilde{\mathbf{E}}}_A$ is known. Using it and the admittance $\hat{\tilde{\boldsymbol{Y}}}_A$, we can calculate the fields $\hat{\tilde{\mathbf{H}}}_A$ and $\hat{\tilde{\mathbf{E}}}_B$ by (73) and (72), respectively. The other quantities, including the surface current density $\hat{\mathbf{S}}_M$, can then be determined by (70).

D. Microstrip Sharp Bends

In this subsection, we would like to analyze sharp microstrip bends (see Fig. 5) by using the algorithm developed before and discretization lines of different lengths. Since the propagation direction changes from z to z', we must restrict the components in the diagonal anisotropic material tensors to $\nu_{xx} = \nu_{zz}$, whereas ν_{yy} can be different from these values.

The tangential fields in the tilted plane E are given by

$$\hat{\mathbf{E}}_t^{\mathrm{I,II}} = \begin{bmatrix} \hat{\mathbf{E}}_y^{\mathrm{I,II}} \\ \hat{\mathbf{E}}_x^{\mathrm{I,II}}\cos(\alpha/2) \pm \hat{\mathbf{E}}_z^{\mathrm{I,II}}\sin(\alpha/2) \end{bmatrix} \tag{75}$$

$$\hat{\mathbf{H}}_t^{\mathrm{I,II}} = \begin{bmatrix} \hat{\mathbf{H}}_x^{\mathrm{I,II}}\cos(\alpha/2) \pm \hat{\mathbf{H}}_z^{\mathrm{I,II}}\sin(\alpha/2) \\ \hat{\mathbf{H}}_y^{\mathrm{I,II}} \end{bmatrix}. \tag{76}$$

The waveguide parts of the bend are labeled I and II. Therefore, we use x and z in waveguide II (instead of x' and z'). The components in the propagation directions are obtained from (7),

which have to be discretized. Matching the tangential electric and magnetic fields in plane E, we obtain ($t_\alpha = \tan(\alpha/2)$)

$$\begin{bmatrix} \hat{\mathbf{E}}_y^{\mathrm{I}} \\ \hat{\mathbf{E}}_x^{\mathrm{I}} \end{bmatrix} - \begin{bmatrix} \hat{\mathbf{E}}_y^{\mathrm{II}} \\ \hat{\mathbf{E}}_x^{\mathrm{II}} \end{bmatrix} = \begin{bmatrix} \mathbf{0} & \mathbf{0} \\ \hat{\boldsymbol{Z}}_{xx} & \hat{\boldsymbol{Z}}_{xy} \end{bmatrix} \begin{bmatrix} -\left(\hat{\mathbf{H}}_x^{\mathrm{I}} + \hat{\mathbf{H}}_x^{\mathrm{II}}\right) \\ \hat{\mathbf{H}}_y^{\mathrm{I}} + \hat{\mathbf{H}}_y^{\mathrm{II}} \end{bmatrix} \tag{77}$$

$$\begin{bmatrix} -\hat{\mathbf{H}}_x^{\mathrm{I}} \\ \hat{\mathbf{H}}_y^{\mathrm{I}} \end{bmatrix} - \begin{bmatrix} -\hat{\mathbf{H}}_x^{\mathrm{II}} \\ \hat{\mathbf{H}}_y^{\mathrm{II}} \end{bmatrix} = \begin{bmatrix} \hat{\boldsymbol{Y}}_{xy} & \hat{\boldsymbol{Y}}_{xx} \\ \mathbf{0} & \mathbf{0} \end{bmatrix} \begin{bmatrix} \hat{\mathbf{E}}_y^{\mathrm{I}} + \hat{\mathbf{E}}_y^{\mathrm{II}} \\ \hat{\mathbf{E}}_x^{\mathrm{I}} + \hat{\mathbf{E}}_x^{\mathrm{II}} \end{bmatrix} \tag{78}$$

where we defined impedance and admittance matrices according to

$$\begin{aligned} \hat{\boldsymbol{Z}}_{xx} &= jt_\alpha \hat{\boldsymbol{M}}_x^{\square} \boldsymbol{\epsilon}_{zz}^{-1} \hat{\boldsymbol{D}}_{\bar{y}}^{\bullet} \\ \hat{\boldsymbol{Z}}_{xy} &= jt_\alpha \hat{\boldsymbol{M}}_x^{\square} \boldsymbol{\epsilon}_{zz}^{-1} \hat{\boldsymbol{D}}_{\bar{x}}^{\circ} \\ \hat{\boldsymbol{Y}}_{xy} &= jt_\alpha \hat{\boldsymbol{M}}_x^{\diamond} \boldsymbol{\mu}_{zz}^{-1} \hat{\boldsymbol{D}}_{\bar{x}}^{\bullet} \\ \hat{\boldsymbol{Y}}_{xx} &= -jt_\alpha \hat{\boldsymbol{M}}_x^{\diamond} \boldsymbol{\mu}_{zz}^{-1} \hat{\boldsymbol{D}}_{\bar{y}}^{\circ}. \end{aligned} \tag{79}$$

We have introduced interpolation matrices $\boldsymbol{M}_x^{\square,\diamond}$ between the discretization line systems. The combination of the above equations yields the following matching relation:

$$\hat{\boldsymbol{P}}_E^{\mathrm{I}} \begin{bmatrix} \hat{\mathbf{E}}_E^{\mathrm{I}} \\ \hat{\mathbf{H}}_E^{\mathrm{I}} \end{bmatrix} = \hat{\boldsymbol{P}}_E^{\mathrm{II}} \begin{bmatrix} \hat{\mathbf{E}}_E^{\mathrm{II}} \\ \hat{\mathbf{H}}_E^{\mathrm{II}} \end{bmatrix} \tag{80}$$

with

$$\hat{\boldsymbol{P}}_E^{\mathrm{I,II}} = \begin{bmatrix} \hat{\boldsymbol{I}}^{\bullet} & & \mp\hat{\boldsymbol{Z}}_{xx} & \mp\hat{\boldsymbol{Z}}_{xy} \\ & \hat{\boldsymbol{I}}^{\circ} & & \\ \mp\hat{\boldsymbol{Y}}_{xy} & \mp\hat{\boldsymbol{Y}}_{xx} & \hat{\boldsymbol{I}}^{\bullet} & \\ & & & \hat{\boldsymbol{I}}^{\circ} \end{bmatrix}. \tag{81}$$

Therefore, the transfer matrix relation between both sides of plane E is given by

$$\begin{bmatrix} \hat{\mathbf{E}}_E^{\mathrm{I}} \\ \hat{\mathbf{H}}_E^{\mathrm{I}} \end{bmatrix} = \left(\hat{\boldsymbol{P}}_E^{\mathrm{I}}\right)^{-1} \hat{\boldsymbol{P}}_E^{\mathrm{II}} \begin{bmatrix} \hat{\mathbf{E}}_E^{\mathrm{II}} \\ \hat{\mathbf{H}}_E^{\mathrm{II}} \end{bmatrix} = \begin{bmatrix} \hat{\boldsymbol{V}}_E^E & \hat{\boldsymbol{Z}}_E^E \\ \hat{\boldsymbol{Y}}_H^E & \hat{\boldsymbol{V}}_H^E \end{bmatrix} \begin{bmatrix} \hat{\mathbf{E}}_E^{\mathrm{II}} \\ \hat{\mathbf{H}}_E^{\mathrm{II}} \end{bmatrix}. \tag{82}$$

Defining impedances on both sides of plane E by $\hat{\mathbf{E}}_E^{\mathrm{I,II}} = \hat{\boldsymbol{Z}}_E^{\mathrm{I,II}} \hat{\mathbf{H}}_E^{\mathrm{I,II}}$, the impedance transformation from sides II to I yields

$$\hat{\boldsymbol{Z}}_E^{\mathrm{I}} = \left(\hat{\boldsymbol{V}}_E^E \hat{\boldsymbol{Z}}_E^{\mathrm{II}} + \hat{\boldsymbol{Z}}_E^E\right)\left(\hat{\boldsymbol{Y}}_H^E \hat{\boldsymbol{Z}}_E^{\mathrm{II}} + \hat{\boldsymbol{V}}_H^E\right)^{-1}. \tag{83}$$

With the help of the transfer matrix relations in (39), we can write the original fields in plane E as functions of the transformed fields in plane $B \equiv B^{\mathrm{I}}$ or $A \equiv A^{\mathrm{I}}$, respectively, as follows:

$$\begin{bmatrix} \hat{\mathbf{E}}_E^{\mathrm{II}} \\ \hat{\mathbf{H}}_E^{\mathrm{II}} \end{bmatrix} = \begin{bmatrix} \hat{\boldsymbol{V}}_E & \hat{\boldsymbol{Z}}_E \\ \hat{\boldsymbol{Y}}_H & \hat{\boldsymbol{V}}_H \end{bmatrix} \begin{bmatrix} \hat{\tilde{\mathbf{E}}}_B \\ \hat{\tilde{\mathbf{H}}}_B \end{bmatrix} \tag{84}$$

$$\begin{bmatrix} \hat{\mathbf{E}}_E^{\mathrm{I}} \\ \hat{\mathbf{H}}_E^{\mathrm{I}} \end{bmatrix} = \begin{bmatrix} \hat{\boldsymbol{V}}_E & -\hat{\boldsymbol{Z}}_E \\ -\hat{\boldsymbol{Y}}_H & \hat{\boldsymbol{V}}_H \end{bmatrix} \begin{bmatrix} \hat{\tilde{\mathbf{E}}}_A \\ \hat{\tilde{\mathbf{H}}}_A \end{bmatrix}. \tag{85}$$

Due to different line length, we have

$$\begin{aligned} \hat{\boldsymbol{V}}_{E,H} &= \hat{\boldsymbol{T}}_{E,H} \bullet \cosh\left(\hat{\tilde{\mathbf{d}}}\boldsymbol{\Gamma}^r\right) \\ \hat{\boldsymbol{Z}}_E &= \hat{\boldsymbol{T}}_E \bullet \sinh\left(\hat{\tilde{\mathbf{d}}}\boldsymbol{\Gamma}^r\right)\hat{\tilde{\boldsymbol{Z}}}_0 \\ \hat{\boldsymbol{Y}}_H &= \hat{\boldsymbol{T}}_H \bullet \sinh\left(\hat{\tilde{\mathbf{d}}}\boldsymbol{\Gamma}^r\right)\hat{\tilde{\boldsymbol{Y}}}_0 \\ \hat{\tilde{\mathbf{d}}} &= \left[\left(\boldsymbol{J}_{\bullet}^t\left(\bar{\mathbf{d}}^{\bullet} \otimes \boldsymbol{\Gamma}_y^{\bullet}\right)\right)^t, \left(\boldsymbol{J}_{\circ}^t\left(\bar{\mathbf{d}}^{\circ} \otimes \boldsymbol{\Gamma}_y^{\circ}\right)\right)^t\right]^t. \end{aligned} \tag{86}$$

The multiplication sign "$\bullet$" denotes that the matrices have to be multiplied element by element (array multiplication). Collecting all $\bar{d}_i$ (see Fig. 5) in a column vector, we obtain the column vector $\bar{\mathbf{d}}$. $\boldsymbol{\Gamma}_y^{\circ,\bullet}$ is a column vector of order $N_y^{\circ,\bullet}$ whose elements are units. Matrices $\boldsymbol{J}_{\bullet,\circ}$ are defined as in (11). $\boldsymbol{\Gamma}^r$ is a row vector containing the diagonal elements of $\boldsymbol{\Gamma}$. Therefore, the product $\hat{\tilde{\mathbf{d}}}\boldsymbol{\Gamma}^r$ is a full matrix. To obtain numerically more stable impedance transformation formulas, we determine the z-matrix parameters by

$$\begin{aligned} \tilde{\boldsymbol{z}}_{11}^{\mathrm{II}} &= \tilde{\boldsymbol{z}}_{22}^{\mathrm{I}} = \boldsymbol{V}_E \boldsymbol{Y}_H^{-1} \\ \tilde{\boldsymbol{z}}_{12}^{\mathrm{II}} &= \tilde{\boldsymbol{z}}_{21}^{\mathrm{I}} = \boldsymbol{V}_E \boldsymbol{Y}_H^{-1} \boldsymbol{V}_H - \boldsymbol{Z}_E \\ \tilde{\boldsymbol{z}}_{22}^{\mathrm{II}} &= \tilde{\boldsymbol{z}}_{11}^{\mathrm{I}} = \boldsymbol{Y}_H^{-1} \boldsymbol{V}_H \\ \tilde{\boldsymbol{z}}_{21}^{\mathrm{II}} &= \tilde{\boldsymbol{z}}_{12}^{\mathrm{I}} = \boldsymbol{Y}_H^{-1}. \end{aligned} \tag{87}$$

The tilde in these parameters indicates that they connect fields in the transform domain on one side and fields in the original domain on the other side of the section. With these matrices, the input impedances in plane E^{II} of section II and plane A^{I} of section I can be calculated by

$$\hat{\boldsymbol{Z}}_E^{\mathrm{II}} = \tilde{\boldsymbol{z}}_{11}^{\mathrm{II}} - \tilde{\boldsymbol{z}}_{12}^{\mathrm{II}}\left(\tilde{\boldsymbol{z}}_{22}^{\mathrm{II}} + \bar{\boldsymbol{Z}}_o^{\mathrm{II}}\right)^{-1} \tilde{\boldsymbol{z}}_{21}^{\mathrm{II}} \tag{88}$$

$$\hat{\boldsymbol{Z}}_A^{\mathrm{I}} = \tilde{\boldsymbol{z}}_{11}^{\mathrm{I}} - \tilde{\boldsymbol{z}}_{12}^{\mathrm{I}}\left(\tilde{\boldsymbol{z}}_{22}^{\mathrm{I}} + \hat{\boldsymbol{Z}}_E^{\mathrm{II}}\right)^{-1} \tilde{\boldsymbol{z}}_{21}^{\mathrm{I}}. \tag{89}$$

In (95), we have introduced the characteristic impedance of the infinitely long waveguide II as a load impedance at port B^{I}. From the input impedance $\hat{\boldsymbol{Z}}_A^{\mathrm{I}}$ and the source mode, the reflected mode and fields can be calculated. Transforming the fields in opposite direction results in the fields at port B^{I} and from those, the scattering parameter S_{21}.

IV. Analysis of Planar Junctions

As an example for the analysis of waveguide junctions in planar technology, we examine the waveguide crossing shown in Fig. 6. The junction region J is bounded by the four ports A–D. In general, waveguides W_A to W_D are connected to these four ports. The connecting waveguides may also differ from the waveguides inside the junction (see, e.g., waveguide W_D). In Fig. 6(b), only the junction region is sketched. Between ports A and B, we have three concatenated waveguide Sections I–III. The ports of these sections are marked by $A^{\mathrm{I}}, B^{\mathrm{I}}$ to $A^{\mathrm{III}}, B^{\mathrm{III}}$. Magnetic boundaries are chosen for the sidewalls of the connecting waveguides. Therefore, we describe the relation of the

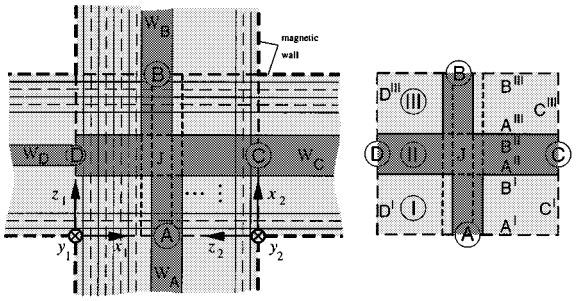

Fig. 6. (a) Junction of planar waveguides. (b) Inner junction.

field at the inner side of the four generalized ports A–D by open-circuit matrix parameters in the form

$$\begin{bmatrix} \hat{\tilde{\mathbf{E}}}_{AB} \\ \hat{\tilde{\mathbf{E}}}_{CD} \end{bmatrix} = \begin{bmatrix} \hat{\tilde{\boldsymbol{z}}}_{AB}^{AB} & \hat{\tilde{\boldsymbol{z}}}_{AB}^{CD} \\ \hat{\tilde{\boldsymbol{z}}}_{CD}^{AB} & \hat{\tilde{\boldsymbol{z}}}_{CD}^{CD} \end{bmatrix} \begin{bmatrix} \hat{\tilde{\mathbf{H}}}_{AB} \\ \hat{\tilde{\mathbf{H}}}_{CD} \end{bmatrix}. \tag{90}$$

The fields at the opposite ports are combined in supervectors, i.e.,

$$\begin{aligned} \hat{\tilde{\mathbf{E}}}_{AB} &= \left[\hat{\tilde{\mathbf{E}}}_A^t, \hat{\tilde{\mathbf{E}}}_B^t \right]^t \\ \hat{\tilde{\mathbf{H}}}_{AB} &= \left[\hat{\tilde{\mathbf{H}}}_A^t, -\hat{\tilde{\mathbf{H}}}_B^t \right]^t. \end{aligned} \tag{91}$$

The four matrices in (90) are obtained by open circuiting the ports. By open circuiting ports C and D, the matrices $\hat{\tilde{\boldsymbol{z}}}_{AB}^{AB}$ and $\hat{\tilde{\boldsymbol{z}}}_{CD}^{AB}$ are obtained. By open circuiting ports A and B, the matrices $\hat{\tilde{\boldsymbol{z}}}_{CD}^{CD}$ and $\hat{\tilde{\boldsymbol{z}}}_{AB}^{CD}$ can be calculated.

A. Main Diagonal Submatrices

First we would like to demonstrate the determination of the two main diagonal submatrices in (90). Let us start with $\hat{\tilde{\boldsymbol{z}}}_{AB}^{AB}$. We assume that ports C and D are open circuited, which means $\hat{\tilde{\mathbf{H}}}_{CD} = \mathbf{0}$. The field relation between ports A and B is then given by

$$\begin{aligned} \hat{\tilde{\mathbf{E}}}_{AB} &= \hat{\tilde{\boldsymbol{z}}}_{AB}^{AB} \hat{\tilde{\mathbf{H}}}_{AB} \\ \hat{\tilde{\boldsymbol{z}}}_{AB}^{AB} &= \begin{bmatrix} \hat{\tilde{\boldsymbol{z}}}_{AB11}^{AB} & \hat{\tilde{\boldsymbol{z}}}_{AB12}^{AB} \\ \hat{\tilde{\boldsymbol{z}}}_{AB21}^{AB} & \hat{\tilde{\boldsymbol{z}}}_{AB22}^{AB} \end{bmatrix}. \end{aligned} \tag{92}$$

To obtain these four submatrices, we again use the technique of open circuiting the ports. With $\hat{\tilde{\mathbf{H}}}_B = \mathbf{0}$, we obtain the submatrices $\hat{\tilde{\boldsymbol{z}}}_{AB11}^{AB}$ and $\hat{\tilde{\boldsymbol{z}}}_{AB21}^{AB}$. $\hat{\tilde{\boldsymbol{z}}}_{AB11}^{AB}$ is the input impedance matrix at the port A^{I} for open port B. In our example, ports A and B are connected via a concatenation of three different waveguide sections. For each of these sections, the tangential fields at the ends of the ports are described by equations as (37). For the transition between the waveguide sections, (57) holds. The input impedance of Section III in plane A^{III} is obtained from the formula in (43) as $\hat{\tilde{\boldsymbol{z}}}_1^{\mathrm{III}}$. From $\hat{\tilde{\boldsymbol{Z}}}_A^{\mathrm{III}} = \hat{\tilde{\boldsymbol{z}}}_1^{\mathrm{III}}$, we obtain with the help of (37) and (57) all impedances at the subports. For the calculation of the matrix $\hat{\tilde{\boldsymbol{z}}}_{AB21}^{AB}$, we must now proceed in the opposite direction. With the input impedance $\hat{\tilde{\boldsymbol{Z}}}_A^{\mathrm{I}}$, i.e., (37), the matching equations and the already calculated impedances, we obtain all the field vectors at the subports and especially $\hat{\tilde{\mathbf{E}}}_B^{\mathrm{III}} = \hat{\tilde{\mathbf{E}}}_B$. For numerically stable calculations, we use the algorithms described in [12]. From $\hat{\tilde{\mathbf{E}}}_B$, which is a function of $\hat{\tilde{\mathbf{H}}}_A$, the transmittance matrix $\hat{\tilde{\boldsymbol{z}}}_{AB21}^{AB}$ is obtained. The analogous procedure holds for the other two submatrices in (92). Now, $\hat{\tilde{\boldsymbol{z}}}_{AB}^{AB}$ is completely determined. In an analogous way, the submatrix $\hat{\tilde{\boldsymbol{z}}}_{CD}^{CD}$ in (90) is obtained. In this case, ports A and B must be open circuited with $\hat{\tilde{\mathbf{H}}}_{AB} = \mathbf{0}$. We now have five different waveguide sections concatenated between ports C and D (see Fig. 6).

B. Off-Diagonal Submatrices

The off-diagonal submatrices describe the coupling between the ports. The matrix $\hat{\tilde{\boldsymbol{z}}}_{CD}^{AB}$ is defined by the equation

$$\begin{aligned} \hat{\tilde{\mathbf{E}}}_{CD} &= \hat{\tilde{\boldsymbol{z}}}_{CD}^{AB} \hat{\tilde{\mathbf{H}}}_{AB} \\ \hat{\tilde{\boldsymbol{z}}}_{CD}^{AB} &= \begin{bmatrix} \hat{\tilde{\boldsymbol{z}}}_{CD11}^{AB} & \hat{\tilde{\boldsymbol{z}}}_{CD12}^{AB} \\ \hat{\tilde{\boldsymbol{z}}}_{CD21}^{AB} & \hat{\tilde{\boldsymbol{z}}}_{CD22}^{AB} \end{bmatrix} \end{aligned} \tag{93}$$

which is obtained from (90) under the condition $\hat{\tilde{\mathbf{H}}}_{CD} = \mathbf{0}$. The submatrices on the left-hand (right-hand) side are obtained by setting $\hat{\tilde{\mathbf{H}}}_B = \mathbf{0}$ ($\hat{\tilde{\mathbf{H}}}_A = \mathbf{0}$). We will now describe the procedure for the two submatrices on the left-hand side. The procedure for the right-hand side submatrices is analogous. Only the electric-field components are responsible for the coupling from ports A and B to ports C and D. The magnetic field produces only zero tangential magnetic-field components at the boundaries C and D (because of the magnetic walls). Thus, we have to determine $\hat{\tilde{\mathbf{E}}}_y^{C,D}$ and $\hat{\tilde{\mathbf{E}}}_z^{C,D}$ caused by $\hat{\tilde{\mathbf{H}}}_A$. These calculations must be performed for the different subports. This is because each of the ports C and D must be partitioned in (in our example, three) subports C^k and D^k according to the sidewalls areas of the waveguide sections. In each of the subports, the calculations for the components have to be performed analogously to rectangular waveguide junctions described in [12]. The required field components at subports A^k and B^k were determined in the previous subsection. From the tangential electric-field components at the subports C^k, D^k, which are proportional to $\hat{\tilde{\mathbf{H}}}_A$, the matrices $\hat{\tilde{\boldsymbol{z}}}_{CD11}^{AB}$ and $\hat{\tilde{\boldsymbol{z}}}_{CD21}^{AB}$ are obtained. In an analogous way, the off-diagonal submatrix $\hat{\tilde{\boldsymbol{z}}}_{AB}^{CD}$ has to be determined.

V. Numerical Results

Numerical results compared with those of other methods showed the accuracy of the proposed algorithm [19]. Further results computed for special devices here are presented to show the wide applicability of the proposed algorithm. Fig. 7 is a plot of the dispersion curves of a microstrip on anisotropic substrate. The dashed lines were obtained by an algorithm with one-dimensional discretization [9]–[11]. These curves are the most accurate ones and can be used as a reference. The thin lines are from [2] with discretization lines in the vertical (y)-direction. The thick lines were obtained using (29). By using a high number of discretization points, the thick lines are very close to the dashed lines. At higher frequencies, the field is more concentrated near the strip. Therefore, these curves

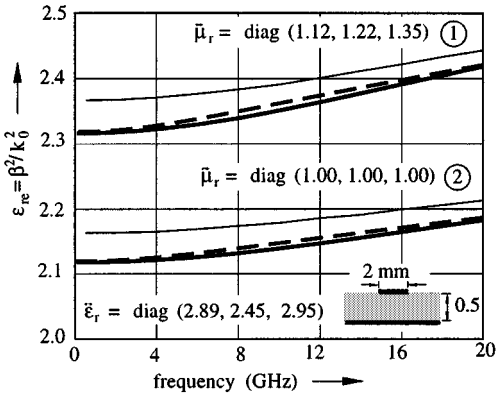

Fig. 7. Dispersion curves of a microstrip on an anisotropic substrate. —: [2], - - -: [10], —: this algorithm.

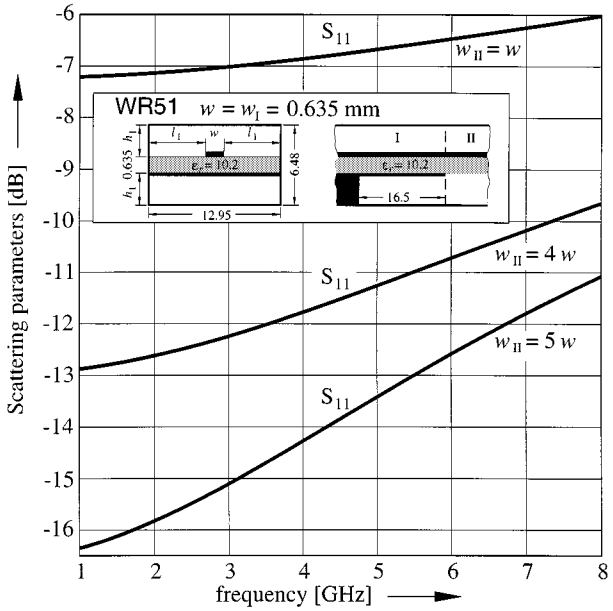

Fig. 8. Scattering parameters $|S_{11}|$ as function of frequency in a waveguide junction (see Fig. 4).

converge toward the same values. This should also be true for the thin lines if the number of discretization lines is increased. Numerical results for the scattering parameters of a transition microstrip/suspended substrate line in a rectangular waveguide WR51 are given in Fig. 8. For the calculations, the formulas of Section III-C were used. As can be seen, the reflections can be reduced by using a larger strip width in waveguide II. Fig. 9 shows numerical results for the reflection coefficient of a microstrip sharp bend as a function of frequency parameterized with the bend angle. In case of the dashed lines, the substrate has anisotropic behavior. The results marked by a ∘ were obtained by a magnetic-wall model and one-dimensional discretization [17]. A 90° bend constructed by concatenation of sharp bends of smaller angles was analyzed (see Fig. 10). As can be seen, in this way, 90° bends can be constructed with a total reflection coefficient smaller than 0.05 in the whole frequency range. For the analysis of microstrip meander lines, Floquet's theorem was introduced into the difference operators. In Fig. 11, dispersion curves for a microstrip meander line are

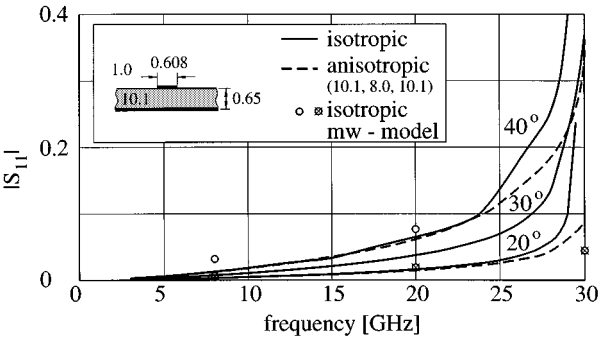

Fig. 9. Scattering parameter $|S_{11}|$ for a microstrip sharp bend. Substrate thickness $= 0.65$ mm, $w = 0.608$ mm, —: $\varepsilon_r = 10.1$, - - - $\epsilon_r^{\leftrightarrow} = \mathrm{diag}(10.1, 8.0, 10.1)$, ∘ from [17].

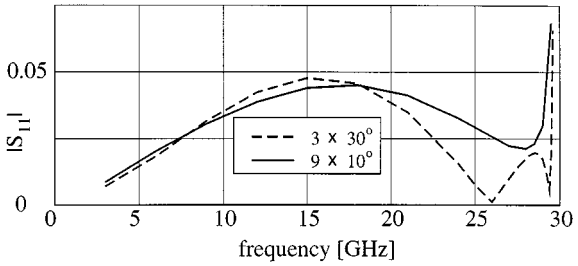

Fig. 10. Scattering parameter $|S_{11}|$ for concatenated sharp microstrip bends to form a 90° bend. Dimensions of the microstrip are as in Fig. 9.

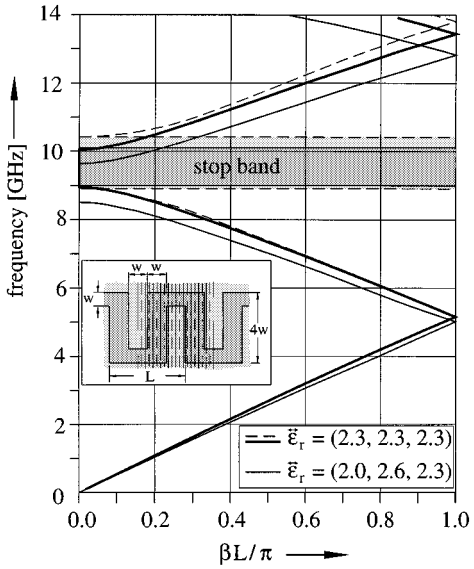

Fig. 11. Dispersion curves for a microstrip meander line. Substrate thickness $= 0.79$ mm, $w = 2.37$ mm, $\varepsilon_r = 2.3$.

shown. The dashed curve is from [20]. The full thick line was obtained with the algorithm described here. The thin line is for an anisotropic substrate. The arithmetic mean value of the permittivities is equal to that of the isotropic case.

VI. Conclusion

A new algorithm based on GTL equations and impedance/admittance transformations has been presented for the analysis of complex planar microwave circuits on anisotropic substrates. The algorithm has been verified by numerical results.

ACKNOWLEDGMENT

The author would like to acknowledge his FernUniversität colleagues S. Helfert, for the help in preparing this paper's manuscript, and L. Greda, for calculating the numerical results of Fig. 8.

REFERENCES

[1] R. Pregla and W. Pascher, "The method of lines," in *Numerical Techniques for Microwave and Millimeter Wave Passive Structures*, T. Itoh, Ed. New York: Wiley, 1989, pp. 381–446.

[2] Y. Chen and B. Beker, "Study of microstrip step discontinuities on bianisotropic substrates using the method of lines and transverse resonance technique," *IEEE Trans. Microwave Theory Tech.*, vol. 42, pp. 1945–1950, Oct. 1994.

[3] L. B. Felsen and N. Marcuvitz, *Radiation and Scattering of Waves*. Piscataway, NJ, USA: IEEE Press, 1996.

[4] V. K. Tripathi, "On the analysis of symmetrical three-line microstrip circuits," *IEEE Trans. Microwave Theory Tech.*, vol. MTT-25, pp. 726–729, Sept. 1977.

[5] R. Pregla, "The impedance/admittance transformation—An efficient concept for the analysis of optical waveguide structures," in *Integrated Photon. Res. Topical Meeting*, Santa Barbara, CA, July 1999, pp. 40–42.

[6] ——, "Novel algorithms for the analysis of optical fiber structures with anisotropic materials," in *Int. Transparent Opt. Networks Conf.*, Kielce, Poland, June 1999, pp. 49–52.

[7] ——, "Efficient modeling of conformal antennas," presented at the Millennium Antennas Propagat. Conf., Davos, Switzerland, Apr. 2000, Paper 0682.

[8] Y. Chen and B. Beker, "The method of lines analysis of double-layered or suspended bianisotropic biaxial substrates," *IEEE Trans. Microwave Theory Tech.*, vol. 42, pp. 917–920, May 1994.

[9] R. Pregla, "The analysis of wave propagation in general anisotropic multilayered waveguides by the method of lines," in *Proc. Int. Electromagn. Theory Symp.*, Thessaloniki, Greece, May 1998, pp. 51–53.

[10] ——, "A generalized algorithm for analysis of planar multilayered anisotropic waveguide structures by the method of lines," *Arch. Elektr. Ubertragung*, vol. 52, no. 2, pp. 94–98, Mar. 1998.

[11] ——, "Correction to 'A generalized algorithm for analysis of planar multilayered anisotropic waveguide structures by the method of lines'," *Arch. Elektr. Ubertragung*, vol. 53, no. 1, p. 32, Jan. 1999.

[12] ——, "The method of lines as generalized transmission line technique for the analysis of multilayered structures," *Arch. Elektr. Ubertragung*, vol. 50, no. 5, pp. 293–300, Sept. 1996.

[13] N. Kaneda, Y. Qian, and T. Itoh, "A broad-band microstrip-to-waveguide transition using quasi-Yagi antenna," *IEEE Trans. Microwave Theory Tech.*, vol. 47, pp. 2562–2567, Dec. 1999.

[14] L. Vietzorreck and R. Pregla, "Hybrid analysis of 3-D MMIC elements by the method of lines," *IEEE Trans. Microwave Theory Tech.*, vol. 44, pp. 2580–2586, Dec. 1996.

[15] R. Pregla and L. Vietzorreck, "Analysis of planar circuits by the method of lines using crossed discretization lines," in *Proc. PIERS*, Boston, MA, 1997, p. 766.

[16] R. Pregla, "MoL–BPM method of lines based beam propagation method," in *Methods for Modeling and Simulation of Guided-Wave Optoelectronic Devices, Progress in Electromagnetic Research (PIER 11)*, W. P. Huang, Ed. Cambridge, MA: EMW Publishing, 1995, pp. 51–102.

[17] ——, "Analysis of a bend discontinuity by the method of lines" (in German), *Frequenz*, vol. 45, pp. 213–216, 1991.

[18] L. Vietzorreck and R. Pregla, "Analysis of MMIC junctions and multiports by the method of lines," in *IEEE MTT-S Int. Microwave Symp. Dig.*, Baltimore, MD, 1998, pp. 1547–1550.

[19] R. Pregla, "Analysis of planar microwave and millimeter-wave circuits with anisotropic layers based on generalized transmission line equations and on the method of lines," in *IEEE MTT-S Int. Microwave Symp. Dig.*, vol. I, Boston, MA, 2000, pp. 125–128.

[20] S. B. Worm and R. Pregla, "Hybrid-mode analysis of arbitrarily shaped planar microwave structures by the method of lines," *IEEE Trans. Microwave Theory Tech.*, vol. MTT-32, pp. 191–196, Oct. 1984.

Reinhold Pregla (M'76–SM'83–F'99) received the Dipl.-Ing. and Dr.-Ing. degrees in electrical engineering from the Technische Universität Braunschweig, Braunschweig, Germany, in 1963 and 1966, respectively.

From 1966 to 1969, he was a Research Assistant in the Department of Electrical Engineering, Institut für Hochfrequenztechnik, Technische Universität Braunschweig, where he was engaged in investigations of microwave filters, group delay equalizers, and electromagnetic field analysis. He was then a Lecturer of high frequencies with the Technische Universität Braunschweig. Since 1973, he has been a Professor with the Ruhr-Universität Bochum, Bochum, Germany. Since 1975, he has been a Full Professor of electrical engineering with the FernUniversität (a university for distance study), Hagen, Germany. He has authored or co-authored approximately 200 papers in international journals and conference proceedings. His fields of research include microwave and millimeter-wave integrated circuits, field theory, antennas and integrated optics, and photonics and he invented the MoL for applications in these fields. He has steadily improved this method and developed it into an efficient analysis and modeling tool.

Dr. Pregla is a member of the IEEE Microwave Theory and Techniques Society (IEEE MTT-S) Editorial Board and the Technical Program Committee for the IEEE MTT-S International Microwave Symposium. He is also a member of the Editorial Board of the IEEE TRANSACTIONS ON MICROWAVE THEORY AND TECHNIQUES.